Towards Sustainable Ultrafast Molecular-Separation Membranes: from Conventional Polymers to Emerging Materials

Towards sustainable ultrafast molecular-separation membranes: From conventional polymers to emerging materials

Xi Quan Cheng[a, e]

Zhen Xing Wang[a, f]

Xu Jiang[a]

Tingxi Li[g]

Cher Hon Lau[b, *]

cherhon.lau@ed.ac.uk

Zhanhu Guo[c, *]

zguo10@utk.edu

Jun Ma[d, e, *]

majun@hit.edu.cn

Lu Shao[a, *]

shaolu@hit.edu.cn

[a]MIIT Key Laboratory of Critical Materials Technology for New Energy Conversion and Storage, School of Chemistry and Chemical Engineering, State Key Laboratory of Urban Water Resource and Environment (SKLUWRE), Harbin Institute of Technology, Harbin 150001, PR China

[b]School of Engineering, The University of Edinburgh, The King's Buildings, Mayfield Road, Edinburgh EH9 3JL, Scotland, UK

[c]Integrated Composites Laboratory (ICL), Department of Chemical & Biomolecular Engineering, University of Tennessee, Knoxville, TN 37996, USA

[d]School of Environmental Science and Engineering, Harbin Institute of Technology, Harbin 150001, PR China

[e]School of Marine Science and Technology, Sino-Europe Membrane Technology Institute (It should be School of Science and Technology, Sino-Europe Membrane Technology Research Institute, Harbin Institute of Technology, Weihai 264209, P R China), Harbin Institute of Technology, Weihai 264209 PR China

[f]Department of Chemistry, Nanchang University, Nanchang 330031, PR China

[g]College of Materials Science and Engineering, Shandong University of Science and Technology, Qingdao 266590, PR China

*Corresponding authors at:MIIT Key Laboratory of Critical Materials Technology for New Energy Conversion and Storage, School of Chemistry and Chemical Engineering, State Key Laboratory of Urban Water Resource and Environmen (SKLUWRE), Harbin Institute of Technology, Harbin 150001, P.R. China (L. Shao). ~~School of Environmental Science and Engineering, Harbin Institute of Technology, Harbin 150001, PR China (J. Ma)~~.

Abstract

Ultrafast molecular separation (UMS) membranes are highly selective towards active organic molecules such as antibiotics, amino acids and proteins that are 0.5–5 nm wide while lacking a phase transition and requiring a low energy input to achieve high speed separation. These advantages are the keys for deploying UMS membranes in a plethora of industries, including petrochemical, food, pharmaceutical, and water treatment industries, especially for dilute system separations. Most recently, advanced nanotechnology and cutting-edge nanomaterials have been combined with membrane separation technologies to generate tremendous potential for accelerating the development of UMS membranes. It is therefore critical to update the broader scientific community on the important advances in this exciting, interdisciplinary field. This review emphasizes the unique separation capabilities of UMS membranes, theories underpinning UMS membranes, traditional polymeric materials and nanomaterials emerging on the horizon for advanced UMS membrane fabrication and technical

applications to address the existing knowledge gap. This work includes detailed discussions regarding existing challenges, as well as perspectives on this promising field.

Keywords: Ultrafast molecular separation (UMS); Polymeric materials; Nanomaterials; Membrane fabrication; Membrane separation

Abbreviations: 2D, 2-dimensional; 3D, 3-dimensional; BCPs, block copolymers; CVD, chemical vapor deposition; COFs, covalent organic framework; DLC, diamond like carbon; EDTA, ethylene diamine tetra acetic acid; EB, Evan's blue; FET, field-effect transistor; GO, graphene oxide; LDHs, layered double hydroxides; MB, methyl blue; MD, molecular dynamics; MOFs, metal organic frameworks; MWCO, molecular weight cut-off; NF, nanofiltration; PBI, polybenzimidazoles; PDMS, polydimethylsiloxane; PSS, poly(sodium 4-styrenesulfonate; PS-b-PMMA, polystyrene-b-poly (methyl methacrylate; PS-b-P4VP, poly (styrene-b-4-vinylpyridine); PEI, polyethylenimine; PAFs, porous aromatic frameworks; PMP, poly(4-methyl-2-pentyne); PI, polyimides; PTMSP, poly[1-(trimethylsilyl)-1-propyne]; PIM, polymer intrinsic microporosity; Rh B, Rhodamine B; SWCNTs, single wall carbon nanotubes; SRNF, solvent-resistant nanofiltration; SPEK, sulfonated polyetherketone; TMOs, transition metal oxides; TMDs, transition metal dichalcogenides; WS_2, tungsten disulfide; UF, ultrafiltration; UMS, ultrafast molecular-separation

1 Introduction

Separation processes are fundamental in the biopharmaceutical, food, agricultural, chemical and petrochemical industries. Traditional separation techniques commonly used in these industries include distillation, pressure- and temperature-swing adsorption, and extraction. These technologies have high carbon footprints and are energy intensive. Compared with traditional separation technologies, membrane separation is more attractive due to its low carbon footprint, small spatial requirements and a lack of a phase transition in most cases [1–17]. In recent years, the impending global energy shortage and various environmental issues have accelerated the development of membrane separation, particularly in membrane assembly using nanotechnology and scale-up translations of membrane science for commercialization [1–17]. Membrane science typically involves chemical synthesis, material science, advanced characterization techniques, membrane manufacturing and modification, module design and process engineering. Therefore, advances in membrane science can simultaneously evolve separation techniques in practical industries and facilitate progression in related science and manufacturing industries.

Membrane separation is typically deployed to extract products (active molecules) from solvents or purify solvents for recycled use. The size of most aqueous organic contaminants and active molecules such as antibiotics, amino acid, dyes and some proteins is between 0.5 and 5 nm. Ideal separation techniques that isolate these molecules are the pore-size-dominated separation processes of nanofiltration (NF) and ultrafiltration (UF) [7–11]. In these processes, solutes are separated from aqueous solutions and organic media. Conventional molecular-sieving NF/UF membranes are fabricated using thick layers of selective polymeric materials with low porosities and broad pore size distributions, limiting their applications [18–22]. Based on the Hagen-Poiseuille equation, the solution flux is proportional to the pressure difference across the membrane and the porosity, and it is inversely proportional to the membrane thickness [23]. Therefore, the thickness and porosity of the selective layer are critical for obtaining polymeric membranes with high flux. Ultrathin membranes with additional passageways for molecular transportation can be fabricated by a combination of advanced nanotechnology, contemporary membrane materials, membrane fabrication strategies, and emerging engineering processes. The 0.5—5 nm pore size of these membranes is ideal for separating/removing organic molecules from water or solvents. As these membranes are usually deployed for separating dilute solutions, the solvent permeances (solvent flux) of such membranes are several orders of magnitudes higher than commercial membranes [24–73] with comparable rejection under standard operating conditions and have attracted significant attention. Considering the features of this class of membranes, we named these membranes as ultrafast molecular separation (UMS) membranes for consistency in the current work. With improvements in separation efficiency, UMS membranes can replace traditional energy-intensive separation processes, especially for very dilute system separations with negligible concentration polarization. Potentially, UMS membranes can also become the mainstay separation technique for technologically important fields such as wastewater treatment, fine chemical separation, food processing, and pharmaceutical production. Hence, it is critical to update the scientific community on such advances. This review starts with the most important aspects of UMS membranes with unique pore sizes ranging from 0.5—to 5 nm, including their properties and unique advantages, followed by a detailed discussion on the theory underpinning ultrafast molecular transport. Through comparisons with traditional fabrication techniques, crucial fabrication approaches for UMS membranes is discussed in the next section. A further chapter discusses in detail membrane materials, particularly emerging 2D materials. Developing perspectives and the critical challenges of UMS membranes are discussed in the last session. This covers promising membrane materials, advanced membrane modules, the validity of existing membrane separation models for UMS membranes and scale-up challenges.

2 Separation properties and the theory behind UMS membranes

2.1 UMS membrane properties and advantages

Different from conventional liquid separation membranes, the distinctive properties of UMS membranes are produced through a unique combination of material choices and fabrication techniques. The rapid development of UMS membranes is aided by building on the principles of basic membrane properties. As shown in Fig. 1, typical UMS membranes consist of a nanometer-thin, highly porous selective layer that is supported on special substrate layers to maintain mechanical stability for commercial applications. Crucial for separating dilute organic solute solutions, UMS membranes can reject more than 90% of molecules with molecular weights ranging from 500 g mol^{-1} to

10,000 g mol^{-1}. This high rejection rate is accompanied with ultrafast permeance that is several orders of magnitude higher than that of conventional/commercial UF and NF membranes. It is inconceivable for conventional separation membranes to achieve molecular transportation as quick as UMS membranes while maintaining high selectivity. This distinct characteristic of UMS membranes facilitates sustainable separation with a significantly lower energy consumption throughout the separation process. A comparison of NF or UF separation between UMS membranes and conventional membranes in Table 1 [24–73] clearly demonstrates the ultrafast permeance (water or solvent) of UMS membranes. Despite the unreliability and instability of graphene oxides and other emerging 2D materials, a majority of UMS membranes are achieved using these nanomaterials [32–56,58,74–77].

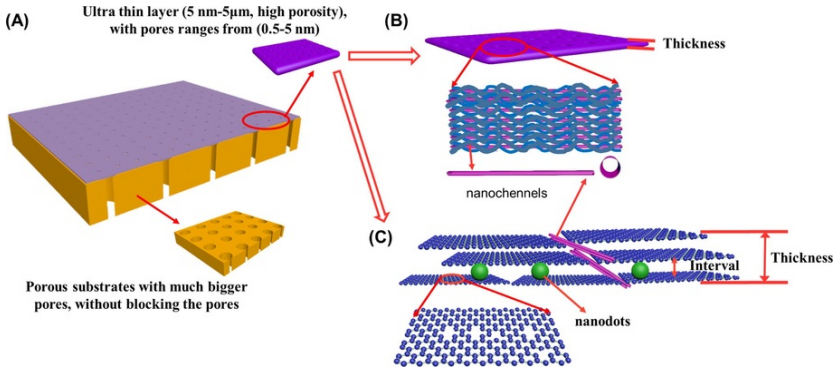

Fig. 1 (A) Structure of ultrafast molecular separation membranes and the ways to facilitate the water or solvent passing through the selective layer of UMS polymeric membranes (B) and 2D material-based UMS membranes (C). For polymeric membranes, the main way to facilitate the water or solvent passing through the UMS membranes is to build an ultrathin selective layer and build nanochannels [24–29,57], since polymeric membranes are soft and. For 2D material-based UMS membranes, it is easier to accelerate the permeance through etching pores on lamellar layers, enlarging the interval between each lamellar layer through the incorporation of nanotubes or nanodots, adjusting the whole thickness of the selective layer, tailoring the size of each lamellar layer and building nanochannels [32–37,52–56,58,74–77].

Table 1 Performance of commercial NF and UF membranes and the state of the art UMS membranes.

Trade name (membrane type)	Manufacture/author	Materials	Thickness (nm)	MWCO (Da) (rejection, -%)	Operation pressure (bar)	Feed concentration (ppm)	Solvent permeance (L m^{-2} h^{-1} bar^{-1})	Solvent permeability (L m^{-2} h^{-1} bar^{-1} m) * 10^{-6}	Ref.
SelRO®/NF	Koch	Hydrophilic (PDMS-based)	Unknown	250–700	30	100	0.5–2.0 (methanol); <1.5 (water)	–	[64,65]
Starmem™ NF	W.R. Grace-Davison	Polyimide based	Unknown	200–400	30	NG	0.16 (hexane), about 0.8 (2-ropanol)	–	[66,67]
SolSep/NF	SolSep BV	Unknown material	Unknown	Not specified	20	NG	0.25 (hexane), <0.1 (ethanol)	–	[68]
DuraMem™/NF	SolSep BV	Unknown material	Unknown	150–500	20/30	25,000/2900	0.2–0.6 (THF), 0.08 (water)	–	[69,70]
GMT-oNF-2/NF	Borsig Membrane Technology	Silicone polymer-based	Unknown	327	30	11000	Unknown	–	[71]
Desal/NF	GE	Polyamide based	Unknown	200–350	20	25000	1.3–4.0 (water)	–	[72,73]
Biomax 100/UF	Millipore	Polyethersulfone	Unknown	50–00 k	NG	NG	688.9–1377.5 (water)	–	–[a]
HFM/UF	Koch	PVDF	Unknown	50–100 k	NG	NG	147.9–493 (water)	–	–[a]

EW/UF	GE Osmonics	Polysulfone	Unknown	100 k	NG	NG	295.8 (water)	–	–[a]
UE50/UF	TriSep	Polyethersulfone	Unknown	100 k	NG	NG	123.3 (water)	–	–[a]
PLHK/UF	Millipore	Regenerated cellulose	Unknown	100 k	NG	NG	435.1 (water)	–	–[a]
Q0100/UF	Advantech	Polysulfone	Unknown	10 k (DY, 3%)	1	<2	Unknown	–	[26]
PLBC (CC)/UF	Millipore	Regenerated cellulose	Unknown	Protoporphyrin (MW = 562.7) (53–84%)	1	<2	4–9 (water)	–	[26]
PLAC/NF	Millipore	Regenerated cellulose	Unknown	Protoporphyrin (100%)	1	<2	Extremely low	–	[26]
UMS (NF)	Gorgojo and Livingston et al.	Polymer with intrinsic microporosity	140	600	15	10 (hexaphenylbenzene)	~18 (n-heptane)	2.52	[24]
UMS (UF)	Deng and Zhang et al.	Sulfonated polyetherketone with cardo groups	414	Cyt.c (MW = 12400), (93%)	0.8	20	1417 (water)	586	[25]
UMS (NF)	Peng et al.	Cross-linked ferritin	60	Direct yellow (DY) (MW = 864.9), (99%)	0.2	<2	9000 (water)	540	[26]
UMS (UF)	Zhang et al.	Cross-linked polystyrene nanoparticles	80	Cyt. C, (100%)	0.8	20	230 (water)	18.4	[27]
UMS (UF)	Shi et al.	Gelatin	165	Cyt. C, (99%), DY, (73%)	1	8.6 (DY) 250 (Cyt.C)	667 (water)	110.1	[28]
UMS (UF)	Whang et al.	P4VP	39	Cyt. C, 95%	0.8	20	580 (water)	22.6	[29]
UMS (NF)	Karan et al.	Diamond-like carbon	35	Protoporphyrin, (99%)	0.8	28	~88 (ethanol)	3.08	[31]
UMS (NF)	Han et al.	Graphene	22	Methyl blue (MB) (MW = 799.8), (99%)	1	16	21.8 (water)	0.48	[32]
UMS (NF)	Qiu	Graphene oxide	Unknown	Unknown	1	8.7	41 (water)	–	[33]
UMS (NF)	Huang	Graphene oxide	2000	Evans blue (EB) (MW = 960.8), (85%)	2	14	71 (water)	142	[34]
UMS (NF)	Ying	Graphene oxide	1080	EB (88%)	1	14	191 (water)	206	[35]
UMS (NF)	Huang	Graphene oxide	1850	Rhodamine B (Rh B) (MW = 479.1) (87%), Evans blue (EB) (83%)	1	EB ~ 14 RB ~ 480	695 (water)	1285	[36]
UMS (NF)	Wang	Graphene oxide	6000	MB (99%)	1	10	428 (water)	2568	[37]
UMS (NF)	Gao	Graphene oxide	40	Rh B, (97.4%)	1	15	720 (water)	28.8	[55]
UMS (NF)	Sun	Laminar MoS_2	1200	EB (89%)	1	14	245 (water)	294	[52]
UMS (NF)	Sun	Laminar WS2	300	EB (90%)	1	14	730 (water)	219	[53]
UMS (NF)	Shi	Reduced Graphene Oxide	18	EB (100%)	1	10	215 (acetone)	3.87	[56]
UMS (NF)	Peinemann	Cellulose	10	Reactive Black-5 (RB5) (MW = 997) (100%)	4	–	700 (water)	7	[57]
UMS (NF)	Qu	Nickel hydroxide nanosheet	3180	DY (97.3%)	0.5	20	99 (water)	314.8	[58]

UMS (NF)	Zhang	ZIF-8/poly(sodium 4-styrenesulfonate)	Unknown	MB (98.6%)	5	100	26.5 (water)	–	[59]
UMS (NF)	Ling	Biomimetic multilayer	~7000	Brilliant Blue G (MW = 883) (100%)	0.8	~115	1250 (water)	8750	[60]
UMS (NF)	Kandambeth	Self-standing COFs	290,000	915	1	1000	180 (acetonitrile)	52200	[61]
UMS (NF)	Ying	GQDs modified thermally Reduced graphene oxide membranes	2340	EB (96%)	1	~10	2000 (water)	4680	[62]
UMS (NF)	Qin	Single-layered graphene	500	342	10	200	50 (water)	25	[63]

[a] Referred from internet: http://www.millipore.com/techpublications/tech1/pf1172en00, http://www.sterlitech.com/flat-sheet-membranes-specifications.html#UF; UMS (UF) means the pores of UMS membranes are in UF range, correspondingly the UMS (NF) means the pore of UMS membranes are in NF range.

The main incentives for developing UF and NF molecular separation membranes are numerous. As a general size-sieving process, no additives are needed, and no phase transition occurs during separation. Compared to distillation, thermal damage is minimized as the low operation temperature prevents degradation and side reactions in membrane materials. There are possibilities for recycling water/solvents and/or valuable compounds, as well as to reduce product loss. It should be noted that the process of active molecular concentration and purification, and water/solvent treatments can be simultaneously achieved during separation [1–4,7–11]. Energy consumption can be reduced by 20% when distillation is replaced by a combination of membrane processes to isolate sulfur-containing hydrocarbon molecules from fluidized catalytic cracking and other naphtha streams. Remarkably, both the product yield and quality can be improved using this combinatory membrane process [10]. Other advantages of UMS membranes for molecular-scale separations include a drastically enhanced separation efficiency, smaller membrane surface area that leads to membrane module miniaturization, and substantial reduction of the operating pressure to separate/purify dilute solutions. Consequently, the cost and energy consumption for industrial-scale, active molecular separation of dilute solutions can be lowered significantly with UMS membranes.

The permeances of UMS membranes are several orders of magnitude higher than those of commercial UF and NF membranes with similar rejection values. It is important to note that this unique combination yields a high permeate product output that is only attainable with dead-end cells in laboratories. It remains nearly impossible to increase permeate purity by several orders of magnitude in real-life applications, where cross-flow separation mode is commonly deployed. This is ascribed to the limitation of feed solution flow-rate, pressure drop and concentration polarization in the membrane modules [78–81]. The energy consumption of separation processes, particularly the desalination of sea water, can be reduced using membranes with permeances of up to $10\,L\,m^{-2}\,h^{-1}\,bar^{-1}$ [1,78,82–84]. Membranes with permeances greater than $10\,L\,m^{-2}\,h^{-1}\,bar^{-1}$ do not lead to further significant reductions in energy consumption. These data were obtained from the separation of concentrated solutions using commercial spiral-wound membrane modules with large surface areas. Therefore, it is clear that the deployment of UMS membranes will distinctively reduce the membrane surface area required for commercial-scale separations. In fact, the reduction of membrane surface area is the major advantage in applying UMS membranes during the separation of active organic molecules in dilute solutions. The total surface area of a membrane module should be optimized to maximize the advantages of UMS membranes.

The membrane surface areas of conventional UF or NF membrane modules (approximately $40\,m^2$ for an 8.0″ × 40″ size module) are too large to maintain a high permeate solution flow-rate. This is due to the complicated mass transfer phenomenon within the module [78–81], pressure drop and concentration polarization. Reducing the membrane surface area not only decreases the capital cost of membrane systems but also benefits mass transfer in the membrane module [79]. In a practical separation process, the membrane surface area drastically impacts the mass transfer within the module. For example, the pressure drop in a spiral-wound module is proportional to the membrane length and solution velocity within the membrane module and is inversely proportional to the membrane width. Shorter membranes reduce the pressure drop across the membrane module, promoting the mass transfer across membranes [79]. Meanwhile, narrower membranes increase the solution velocity within the module [79], diminishing concentration polarization. A significant reduction in membrane surface area may lead to the miniaturization of membrane modules for industrial applications while maximizing separation performance, especially for dilute system separations. When deployed for recycling or the removal of active molecules from dilute solutions (several ppm to several hundreds of ppm), the ultrahigh permeance of UMS membranes can reduce the operating pressure, further reducing energy consumption and other operating costs. In fact, the dilute concentration of the feed solution (from 1 ppm to 250 ppm) in many circumstances [24–63,85–90] results in lower osmotic pressures (the minimum pressure that drives the solution passing through the membrane). Under such circumstances, the low osmotic pressure of the feed solution coupled with the high permeance of a UMS membrane facilitate effective separations at a substantially low pressure (even near 1 bar). For example, when separating a 2 ppm protoporphyrin solution, a commercial membrane (PLBC, NMWL 3000) demonstrated a solution permeance of $10\,L\,m^{-2}\,h^{-1}\,bar^{-1}$ with a protoporphyrin rejection of 53%. If $10\,m^2$ of a conventional membrane is deployed to separate 1000 L of the protoporphyrin solution at 5.0 bar, this process will take 2.0 h (assuming the recovery rate is 100%). Using the same mixture, UMS membranes fabricated from crosslinked ferritin demonstrated a solution permeance as high as $6000\,L\,m^{-2}\,h^{-1}\,bar^{-1}$. This is

approximately 600 times higher than that of commercial membranes while rejecting 100% of the protoporphyrin [26]. This separation can be achieved in 1 h using only 0.17 m^2 of UMS membranes at 1.0 bar. In this case, both the operating pressure and membrane surface area of the UMS membrane were significantly lower/smaller than conventional commercial UF membranes, while the rejection and separating speed of the UMS membrane were substantially higher; these properties could reduce both the cost and the energy consumption of the separation process. In summary, the rapid development of membrane materials and fabrication techniques and the exploration of new dilute system separation applications can generate UMS membranes that will accelerate molecular separations, thereby revolutionizing current membrane manufacturing industries and other related industries, such as module production and system designs.

2.2 Theory behind UMS membranes

Fundamentally, the design of UMS membranes is inspired by basic membrane separation theory. Membrane separation driven by chemical potential gradients such as pressure gradients, temperature gradients and concentration gradients can be analyzed using solution-diffusion or pore-flow models [91–100]. The solution-diffusion model is effective for describing dense membranes without pores or with extremely small pore sizes (less than 0.5 nm) for gas separation, reverse osmosis, dialysis and pervaporation. In the solution-diffusion model, targeted molecules first adsorb on and dissolve into the membrane materials, followed by diffusion across the membrane under a driving force. The pore-flow model is usually applicable to microfiltration (MF), UF or NF membranes containing tiny pores from the nanoscale to microscale. Molecular transportation and screening in these membranes are dominated by pores that are larger than 1 nm. Hence, the pore-flow model is sufficient to guide a detailed analysis of the transportation and separation mechanisms in most UMS membranes where the pore size ranges between 0.5 and 5 nm. However, the molecular transport and separation in UMS membranes with smaller pores in the region of 0.5–1 nm may be related to more complicated models, which are not discussed here.

To analyze molecular transport in UMS membranes using the pore-flow model (Hagen-Poiseuille equation), we first assume that UMS membranes contain a series of cylindrical capillary pores with a diameter of d (m), and the quantity of the liquid (q) flowing through a single pore is defined as:

$$q = (\pi d^4)/128\mu L \cdot \Delta P \quad (1)$$

where μ is the viscosity (Pa (bar) s (h)) of the liquid, L is the length (m) of the cylindrical pore (membrane thickness), and ΔP (bar (Pa)) is the pressure applied across the pore. Assuming equal-sized pores and porosity (ε) in the membrane, the pore number (N) per square centimeter is inversely proportional to the square of d, and N can be calculated as:

$$N = 4 \cdot \varepsilon / \pi d^2 \quad (2)$$

Therefore, by combining Eqs. (1) and (2), the Hagen-Poiseuille equation can be derived as:

$$J = \varepsilon \Delta P d^2 / 32\mu L \quad (3)$$

or

$$J = \varepsilon \Delta P \pi r^2 / 8\mu L \quad (4)$$

where J is the water/solvent flux (L m^{-2} h^{-1}), and r (m) is the pore radius. In most cases, the pores are tortuous (continuous openings), so the Hagen-Poiseuille equation should be modified as:

$$J = \varepsilon \Delta P \pi r^2 / 8\delta\mu L \quad (5)$$

where δ is the membrane tortuosity indicating the ratio of the true flow-path length and the straight-line distance between the beginning and end points [23]. Taking the osmotic pressure of the feed solution into consideration, the equation can be modified as:

$$J = \varepsilon(\Delta P - \Pi)\pi r^2 / 8\delta\mu L \quad (6)$$

where Π represents the osmotic pressure (bar). The assumptions for the above equations are that the fluid is incompressible and Newtonian. In many circumstances, the permeance (L m^{-2} h^{-1} bar^{-1}) is applied to evaluate the membrane, thereby diminishing the effects of pressure, and is defined as

$$Permeance = J/(\Delta P - \Pi) \quad (7)$$

The permeability (L m^{-2} h^{-1} bar^{-1} m) reflects the permeable properties of a membrane with the same thickness as the selective layer (including nanochannels) and is defined as:

$$Permeability = \text{Permeance} \times L \quad (8)$$

By combining Eq. (5) with the Spiegler–Kedem approach and the pore flow model, the solution flux (g m^{-2} h^{-1}), J_s, can be defined as [94,99,100]:

$$J_S = \bar{P}\frac{dc}{dx} + J \cdot C(1-\sigma) \quad \textbf{(9)}$$

where $\bar{P}$ reflects the local solute permeance coefficient, C is the average concentration ($g\,L^{-1}$) of the solute in the membrane, x is the distance across the membrane (m), and σ refers to the reflection coefficient. In addition to the membrane flux, the rejection of a membrane to the contaminants in a solution is another crucial parameter.

The following equation can be used for solute rejection [94]:

$$R \equiv \left(1 - \frac{C_P}{C_B}\right) = \frac{(1-F)\sigma}{1-\sigma F} \quad \textbf{(10)}$$

where R refers to the rejection of solutes, C_P is the permeate concentration ($g\,L^{-1}$), C_B is the feed concentration ($g\,L^{-1}$), and F is defined as:

$$F = \exp\left[-J(1-\sigma)/P_S\right], \text{ and } P_S = \bar{P}/L \quad \textbf{(11)}$$

According to the pore flow model, the membrane flux depends on the porosity, operating pressure, pore diameter and thickness of the selective membrane. However, it is difficult to obtain the accurate thickness and porosity of a selective layer because of the lack of precise characterization techniques, especially when the layer is in the nanometer regime. This hampers the quantitative analysis of mass transfer across membranes. Other factors affecting mass transfer across membranes include the operating pressure, concentration polarization and membrane swelling. The impact of each factor is discussed in the following section.

2.2.1 The effects of membrane properties on the mass transfer across membranes

In practice, the flux represents the output, and rejection refers to product purity during the membrane separation process. An ideal molecular-sieving membrane with a finely tailored pore size (0.5–5 nm) and a high porosity is desired to demonstrate good rejection, while ensuring an ultrahigh flux. Taking only the membrane parameters into consideration, the permeance is exploited to evaluate the mass transfer speed instead of flux. According to the Hagen-Poiseuille equation, the membrane pore size and porosity (i.e., concentration and membrane thickness) are the influential parameters that determine the membrane permeance [23]. In an ideal situation, one should be able to tune each parameter to tailor membrane properties to benefit the targeted application. For example, larger pore radii can significantly boost flux, as it is proportional to the square of the radius, at the expense of selectivity. However, the rejection will decline significantly even with tiny increments in membrane pore size, particularly for discrete nanosized molecules. Hence, the membrane pore size should not be further enlarged. The pore radii of UMS membranes must be deliberately determined by the fabrication process and the size of the targeted species during separation. Membrane pore sizes are rarely uniform and exist mostly as pore size distributions. Targeted molecules may pass through larger pores, whereas smaller pores may limit the transport of water or solvent molecules. Therefore, membranes with a narrow pore size distribution are preferred [101].

The second parameter that influences molecular transport in UMS membranes is porosity. In conventional UF and NF membranes, pores only account for a small fraction of the selective layer. Any changes to porosity will be reflected by alterations to the mean effective pore radius, leading to diminished selectivity. It remains a challenge to increase porosity while maintaining an effective pore size (in the range of 0.5–5 nm) in a defect-free structure. The ability to simultaneously overcome these issues will yield UMS membranes capable of ultrafast water or solvent transport and near 100-% rejection. Recent developments in nanoscience and nanotechnology has enabled the development of inorganic nanotubes and nanofibers. These nanomaterials, a few micrometers in length and approximately 2 nm in diameter, can be deployed as a sacrificial layer to induce additional porosity within conventional membranes for precise pore control [25–29,31,36–37,52–57].

The third parameter that determines transportation rates in UMS membranes is the membrane thickness. Thinner membranes will shorten the length of selective pores, reducing the time required for molecular transport across the membrane. This is a rational and intriguing strategy to maximize water or solvent permeance without compromising the separation capability of membranes. For polymeric materials, the main method to produce high-permeance membranes is to create an ultrathin selective layer or build additional nanochannels. Consequently, UMS membranes fabricated from polymeric membranes typically demonstrate a rejection towards the UF scale (1.5–5 nm) (shown in Fig. 1B and Table 1) [24–29,57,60]. Another approach to reduce membrane thickness is the use of 2D (nano-) materials. These materials provide new possibilities of controlling membrane porosity when fabricating a membrane with a very small mean effective pore size. Unlike polymeric membranes, the permeance and rejection performance of 2D materials can be adjusted by tuning the size of lamellar layers, pore-etching of lamellar layers, functionalization, tailoring the interval distance of the 2D materials, building additional nanochannels for solvents to pass through and regulating the thickness of the selective layer (Fig. 1C). Most UMS membranes fabricated with 2D materials demonstrate permeances as high as 700 $L\,m^{-2}\,h^{-1}\,bar^{-1}$ with dye rejections of approximately 90-% [32–37,52–56,58,62–63].

2.2.2 Other factors affecting the mass transfer across membranes

Other than intrinsic membrane properties, the operational and external factors that affect mass transfer across a membrane include the pressure difference across the membrane (ΔP), concentration polarization, swelling of the membrane, operating temperature, feed solution flow rate, the interaction between solvent and solute, and the interaction between solute and membrane [7–9,11,78–81,102–105]. The latter four parameters are seldom investigated. This section only discusses the effects of pressure, concentration polarization and membrane swelling on the solvent transfer of membranes [7–9,11,78–81,102–105].

ΔP should be higher than the osmotic pressure to provide a driving force to facilitate membrane separation. Large increases in operating pressure can enhance the flux at the expense of higher operating costs, as equipment is required to

pressurize the feed solution. When UMS membranes are deployed to separate dilute feed mixtures, low osmotic pressures are present [24–63,85–90], thus, dispensing the need for a high ΔP. For example, the osmotic pressure in a membrane that is used to separate 100 ppm of a targeted molecule (Mw 500 g mol^{-1}) at 30 °C is only 504 Pa. In a typical NF setting, a high operating pressure (approximately 20–30 bar) is applied across the membrane. This is to accelerate the solvent flux rather than to overcome osmotic pressure. The permeances of UMS membranes are typically a few orders of magnitude better than those of conventional UF/NF membranes, removing the need for high pressures to promote flux acceleration. In fact, only 0.8—1 bar and 0.8—5 bar of pressure are required for UMS membranes during UF and NF operations, respectively; this drastically reduces capital investment for compression equipment and operating costs. Meanwhile, the ultrahigh permeances of UMS membranes void the requirement of a high membrane surface area to achieve the permeation solution flow rates mandatory for processing large mixture quantities.

Concentration polarization is a common phenomenon where the concentration of solutes near a membrane surface is higher than that of the bulk solution. This is ascribed to the solute accumulation as water or solvent passes through the membrane, whereas the solute is blocked during membrane separation. Concentration polarization severely hampers mass transfer as the osmotic pressure around the membrane can be extremely high, resulting in a severe flux decline. Moreover, a larger solute concentration difference across the membrane can reduce rejection [102–105]. Under similar operating conditions and same surface areas, high permeance membranes are more susceptible to concentration polarization than other membranes. Generally, concentration polarization can only be limited, rather than avoided. Faster feed solution flow rates can provide better control over concentration polarization [102–105]. A greener alternative to limit concentration polarization in UMS membranes is to reduce the surface area of each membrane in the membrane module. This differs from the traditional UF or NF membrane design as large surface areas are required to compensate for insufficient permeances to meet application requirements. An appropriate reduction in the surface area of ultrapermeable UMS membranes will not sacrifice the total flow rate of permeate solutions. As mentioned above, coupled with constant feed and permeate solution flow rates, a lower effective membrane surface area will improve the speed of the solution flow while decreasing the pressure drop across the membrane module [79]. This also limits the concentration polarization in spiral-wound and flat-sheet membrane modules. Remarkably, this is attained with less materials and lower membrane cost. As UMS membranes are mainly deployed in the separation of dilute solutions, the concentration polarization is not serious in such circumstances.

Membrane swelling is attributed to the strong interactions between solvents and polymers and impacts the membrane separation performance. Polymer swelling expands the passageways for molecular transport in membranes, thereby sacrificing rejection performance [7,8,11]. Swelling in conventional membranes is typically neglected when applied in aqueous solutions. However, swelling in UMS membranes fabricated from water-soluble polymers should not be neglected, especially in strong solvents, such as DMF, DMSO and chloroform. For example, Wang et al. developed UMS membranes by filtering a PV4P dilute gel solution on polycarbonate substrates. The PV4P selective layers swelled significantly when the membranes were not crosslinked by 1,3-dibromopropane (DBP). After crosslinking, the degree of swelling was halved, and the material exhibited better hydrostability [29]. The prevention of significant swelling in UMS membranes is essential for maintaining high selectivity [7–9,11,29]. UMS membrane swelling can be overcome with crosslinking and the incorporation of nanoparticles [26,28–29]. As UMS membranes are a relatively new research area in membrane science, detailed studies on the impact of swelling on UMS separation performance remains scarce.

3 Preparing UMS membranes

Membrane permeance quantifies the mass transfer velocity across membranes, while rejection can be used to evaluate product purity. The key to preparing USM membranes with excellent separation performance is to construct ultrathin, defect-free selective layers with high porosity [23]. Finding suitable ways to design ultrathin selective layers or build additional liquid-transporting nanochannels is critical to developing USM membranes with excellent separation performance. The construction of additional passageways enhances membrane porosity, promoting the transportation of solvent molecules across the membrane, while ultrathin membranes reduce the time required for molecule transportation [24–63]. We next discuss various UMS membrane fabrication methods. Conventional methods (listed in Fig. 2) such as phase inversion, interfacial polymerization and coating are analyzed to illustrate the limitations and advantages of each method for developing asymmetric and composite UMS membranes [7–9,11]. We also discuss mainstream fabrication methods and promising ways to obtain UMS membranes.

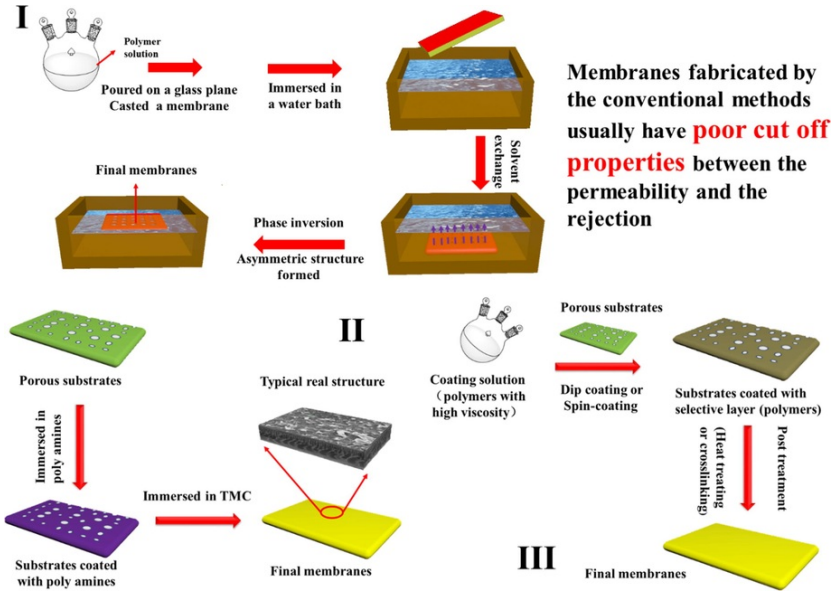

Fig. 2 Processes of conventional methods to fabricate ultrafiltration or nanofiltration membranes: (I) phase inversion, (II) interfacial polymerization, and (III) typical coating process.

3.1 Conventional fabrication approaches

The majority of conventional UF membranes and porous supports of NF membranes are produced through phase inversion [106–110]. Asymmetric membranes are formed when organic solvents containing both polymers and additives (such as pore forming agents) are exchanged with water (Fig. 2I). A high concentration polymer solution (>15%) is typically required to obtain defect-free membranes. The top layer is perceived as the selective layer, which is thicker and less porous [18–22]. Both the sub-layer and the selective layer provide resistance to the solution. High fluxes can be achieved with larger pore sizes, albeit at the expense of rejection. It remains difficult to use the conventional approach of phase inversion to produce highly porous membranes with an ultrathin selective layer. A more suitable approach to construct nanometer-thin selective layers is through interfacial polymerization (IP) [111–114]. IP is also currently the main fabrication route to manufacture commercial NF membranes (Fig. 2II). Challenges using interfacial polymerization include little control over the polymerization degree and the formation of crosslinked network structures, as polymerization occurs quickly. Oligomer formation may block the porous support that subsequently increases solution resistance and the formation of small pores. This process decimates membrane porosity while yielding highly selective membranes for small molecule separation (MWCO 200–500 $g\,mol^{-1}$) but low water permeance (3–20 $L\,m^{-2}\,h^{-1}\,bar^{-1}$) [111–114]. Coating is effective for constructing selective layers of NF membranes while tailoring membrane hydrophilicity. The key advantage of this method is the ease of controlling coating layer thickness. However, coating solutions tend to infiltrate porous supports containing larger pores during the traditional coating process, compromising solution permeation. It remains difficult to simultaneously obtain high porosity and ultrathin selective layers with finely tuned nanoscale pores using conventional UF or NF membrane fabrication processes. As such, membranes obtained from these methods often display poor separation properties or insufficient flux to qualify as UMS membranes.

3.2 Promising strategy to construct ultrathin selective layers - coating

Among traditional ultrathin membrane fabrication techniques, coating is the simplest and most flexible technique for constructing UMS membranes [115,116]. A combinatory approach of phase inversion-coating provides a possible approach to inhibit the infiltration of coating solution into substrate pores while providing deliberate control over the thickness of the coating layer. This approach was used to fabricate polymer intrinsic microporosity (PIM-1) in NF membranes with ultrahigh n-heptane permeance for dye separations (Fig. 3) [24]. Spin-coated PIM-1 membranes were first removed from glass substrates, and then supported on porous substrates. Unlike conventional phase inversion, the PIM-1 concentration in the coating solution was as low as 0.25–2.5 wt%. This is crucial for fabricating 35–600 nm selective layers. The intrinsic high free volume of PIM-1 and the ultrathin (140 nm) defect-free selective layer is the main reason behind an exemplary heptane permeance of 18 $L\,m^{-2}\,h^{-1}\,bar^{-1}$. This is approximately two orders of magnitude higher than that of Starmem 240 (a commercial polyimide-based OSN membrane) with a similar rejection performance [24] and a molecular weight cut-off as low as 500 $g\,mol^{-1}$. Interestingly, the liquid permeance of an ultrathin membrane is substantially lower, contradicting the Hagen-Poiseuille equation. This is attributed to the inherent aging properties of polymer chains when they lose conformation confinement at the ultrathin status [117–122]. The approach to producing ultrathin polymeric films is the typical strategy for yielding UMS membranes.

Hence, the stability of these membranes is a crucial parameter that must be evaluated as well. The high free volume content and excellent film-forming properties of ultrathin dense layers coated from a dilute polymeric/volatile solvent solution are mandatory for producing UMS membranes *via* the phase inversion-coating method. These ultrathin membranes are formed by the phase inversion of polymeric materials that are soluble in volatile solvents and immiscible in water. Other than PIM-1, polymers with a high free volume, such as polydimethylsiloxane (PDMS) and poly[1-(trimethylsilyl)-1-propyne] (PTMSP), are promising for the development of UMS membranes through the phase inversion-coating method.

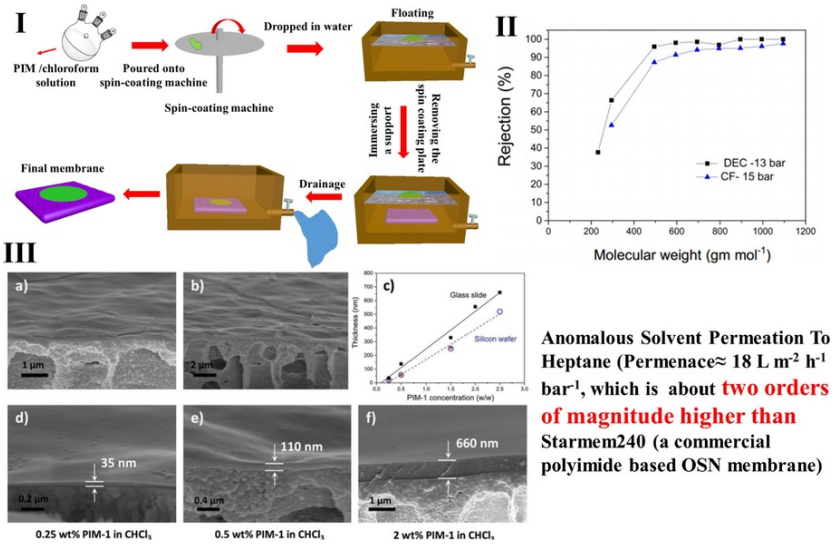

Fig. 3 The preparation of PIM-based UMS membranes and their properties: (I) the preparation process; (II) the molecular weight cut off of PIM-based membranes, DEC: dead end, CF: cross flow; and (III) the concentration-dependent thickness of PIM-1 membranes [24].

Another approach to construct UMS membranes is to combine reduced pressure coating (filtration-coating) with the construction of additional nanochannels (nanoscaled passageways) for water or solvent transportation. A typical UMS membrane fabrication includes the formation of an ultrathin polymer selective-layer on the surface of a sacrificial layer comprised of metal hydroxide nanostrands on the substrate. These nanostrands can also be deployed as pore-forming additives in the polymer coating solution to yield a mixed matrix membrane [25–28,31,37,53–54]. The sacrificial layer and pore-forming additives are usually removed using solutions containing HCl or EDTA to form additional nanochannels for enhanced solvent transport. This results in the ultrafast permeation of solutions (as shown in Fig. 4). Nanostrands are first synthesized [115,116,121–124] and coated on microfiltration membranes with 200 nm pores through filtration. As the length of the nanostrands (approximately a few micrometers) is larger than that of the microfiltration membrane pores, the nanostrands are readily spread on the supports. Upon forming this sacrificial layer of nanostrands, the coating solution is poured onto the microfiltration membranes and filtered under reduced pressure. Alternatively, nanostrands can be mixed with materials that form the selective-layer membrane before filtration. In this case, smaller nanostrands with diameters of approximately 2 nm form pores for molecular screening and/or aid membrane formation with post crosslinking treatments. The thickness of this selective layer can be controlled by the polymer concentration and volume of the applied coating solution [25–28,31,37,53–54]. This process is classified as a coating-etching process in this review.

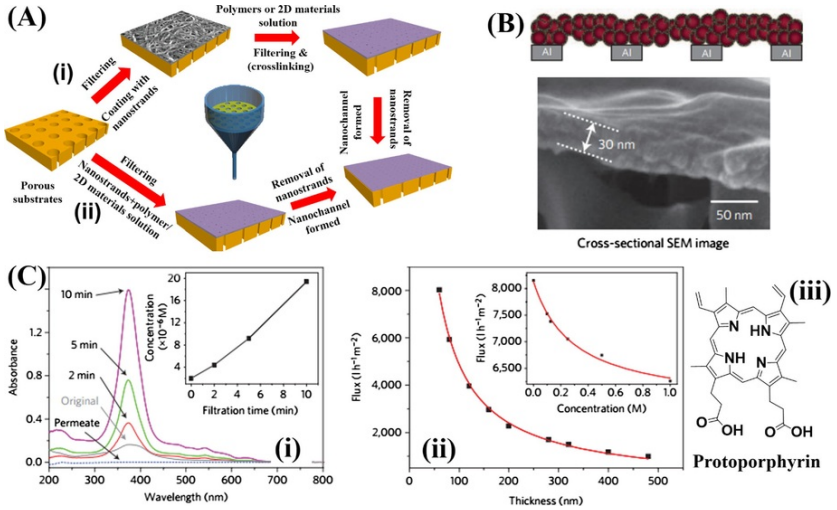

Fig. 4 The fabrication process of UMS membranes through building a sacrificial layer, and the properties of crosslinked ferritin membrane fabricated by the method: (A) the fabrication process: (i) the formation of nanostrand layer first, and then the filtration of polymers combined with crosslinking; (ii) filtrating nanostrands mixed with polymers or two-dimensional materials. (B) The cross-section structure of the crosslinked ferritin membrane [26]. (C) The separation performance of protoporphyrin of the crosslinked ferritin membrane: (i) UV absorbance of the solution before and after filtration; (ii) the thickness-dependent flux of the crosslinked membrane; and (iii) the structure of protoporphyrin [26].

Studies reporting UMS fabrications using polymeric materials remain scarce, yet the superb membrane separation properties of such membranes render them attractive. Most polymeric UMS membranes are developed using the coating-etching method. For instance, Peng and coworkers developed crosslinked ferritin selective layers on a porous polycarbonate membrane using this method [26]. Ferritin was initially mixed with cadmium hydroxide nanostrands in solution before filtration. A membrane was readily formed by subsequent crosslinking with a 10 wt% glutaraldehyde solution for 1 h. Additional passageways with tunable diameters smaller than 2.2 nm for water transport were formed after nanostrand dissolution. By varying the volume of the ferritin/nanostrand solution, the thickness of ferritin membranes was tuned between 30 and 100 nm. By imbuing high porosity and small pore sizes to ultrathin selective layers, the ferritin membranes demonstrated high rejections of protoporphyrin (562.7 g mol^{-1} nearly 100%) and direct yellow (864.9 g mol^{-1}, approximately 99%) with an ultrahigh pure water permeance of 8100 L m^{-2} h^{-1} bar^{-1} (Fig. 4). Compared with commercial membranes, the pure water permeance of this crosslinked ultrathin ferritin membrane was at least 1000 times higher. It is worth noting that the coating solution did not clog the substrate pores, and crosslinking was required to minimize the impact of the polymer solution and swelling in solvents. Gelatin was also used to fabricate UMS membranes with thicknesses ranging from 62 to 250 nm by Shi and coworkers [28]. In their work, copper hydroxide nanostrands were sacrificed to enhance water permeance and prevented the penetration of the polymer solution into substrate pores [28]. SWCNTs were utilized to enhance the mechanical strength of these membranes. Surprisingly, the author claimed that SWCNTs enhanced the flux and rejection rates of the gelatin-based membranes. The tensile strength of the 165 nm gelatin-SWCNTs membrane increased by over 100%, reaching up to 127 MPa. The membrane also exhibited a flux as high as 667 L m^{-2} h^{-1} bar^{-1} alongside a high direct yellow rejection (73%) and a high Cyt. C rejection (99%). Notably, this membrane presented good stability under continuous operation for one week. In addition, the separation performance was retained even after a year's storage in pure water.

Unlike polymers, 2D materials, such as graphene oxide and WS_2, have attracted considerable attention for use in the preparation of UMS membranes. This is due to their ability to yield nanochannels for molecular transport [32–56]. Pore size and concentration (porosity) between the robust structures of 2D materials are tuned easily through the control of nanostrand diameter, introducing a sacrificial layer or the incorporation of nanotubes. Huang and coworkers successfully synthesized a nanostrand-channeled GO (NSC-GO) membrane using copper hydroxide nanostrands as a sacrificial template [36]. Positively charged $Cu(OH)_2$ nanostrands that were 2.5 nm in diameter and micrometers in length were mixed with negatively charged GO solutions. The fine intercalation of $Cu(OH)_2$ nanostrands between GO sheets was achieved through electrostatic attraction. Thereafter, as illustrated in Fig. 5, a nanochanneled network was formed upon acid removal of the copper hydroxide nanostrands. The 2D nanostructures and nanochannels between different layers of GO resulted in a water permeance that was at least 100 times higher than that of commercial membranes. The rejection rate of these high flux membranes was comparable to commercial membranes. These membranes also exhibited excellent mechanical properties under high applied pressures (up to 0.4 MPa) (Fig. 5). By increasing the applied pressure to tailor the elastic deformation of nanochannels, this approach provided possibilities to tailor permeance and rejection rates to suit the stringent requirements of industrial separation applications (Fig. 5 III a). Moreover, MD simulations predicted the quick restoration of deformed nanochannels to their original state.

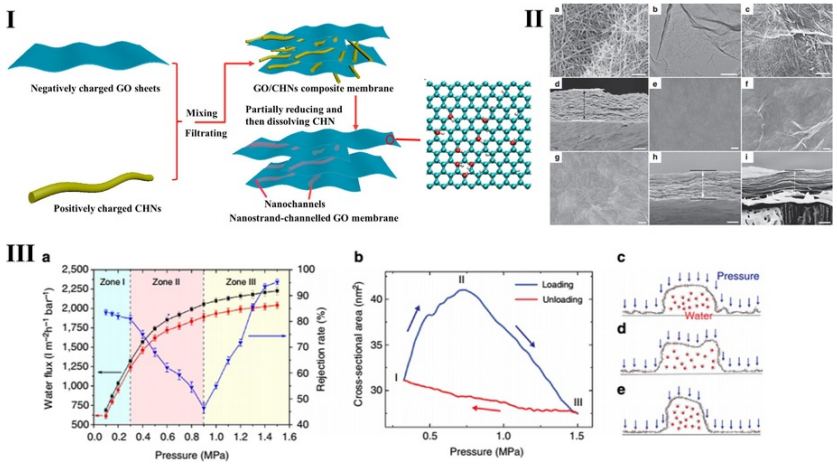

Fig. 5 (I) Process of fabricating nanochannel GO membrane. (II) The structure of nanochannel GO membrane: (a) an SEM image of CHNs (scale bar, 200 nm), (b) TEM image of GO/CHNs composite (scale bar, 500 nm), (c) SEM image of surface of GO/CHNs membrane (scale bar, 100 nm), (d) cross-section of GO/CHNs membrane (thickness, 2.17 mm; scale bar, 1 mm), (e) SEM image of GO/CHNs membrane by direct EDTA treatment (scale bar, 200 nm), (f) SEM image of GO/CHNs membrane treated by N_2H_4 for 15 min (scale bar, 100 nm), (g) SEM image of NSC-GO membrane (scale bar, 200 nm), (h) Cross-sectional view of NSC-GO membrane (thickness, 2.03 mm; scale bar, 1 mm), and (i) cross-sectional view of the GO membrane (thickness, 1.85 mm; scale bar, 1 mm). (III) The response of NSC-GO membranes to the applied pressure: (a Pressure-dependent flux and rejection of EB molecules for the NSC-GO membrane under different pressures. The black solid square and red solid circle curves represent the flux variation during the first and third pressure-loading processes, respectively. The blue solid triangle curv denotes the rejection rate of EB during the first pressure-loading process. All the error bars are average errors from five measurement data. (b) Simulated changes in the cross-sectional area of the nanochannels by varying the applied pressure. (c–e) The response of a half-cylindrica GO nanochannel modeled in an MD simulation [36].

In addition to nanostrands, nanodots and nanotubes have also been deployed to create additional solvent passageways to enhance the porosity of 2D-based membranes [37,55]. By adjusting carbon dot sizes or nanotube diameters between GO layers, the interval between each GO layer can be tuned in a precise manner. Nanoparticle-pillared graphene oxide membranes removed 96–% of dyes from solvents, and membrane permeances reached up to $720\,L\,m^{-2}\,h^{-1}\,bar^{-1}$ [37,55]. Other than carbonaceous nanomaterials, rigid MOF nanotubes were also utilized to increase the interval spacing of the 2D materials and improve solvent permeation to yield novel UMS membranes [125–128]. Ascribing to incompatibility, insoluble nanomaterials are not preferred for the development of polymeric UMS membranes. Polymer chains tend to wrap around insoluble nanotubes or nanodots as they are significantly softer compared with rigid 2D lamellar layers, making it hard to significantly enhance membrane permeance.

3.3 Other potential approaches for UMS fabrications

With the development of advanced manufacturing technologies and bionics, liquid channels can be developed with biomimetic structures [129–135]. This allows the formation of an ultrathin layer through self-assembly, the building of uniform pores with the “breath figure,” and 3D printing. These cutting-edge technologies offer diverse approaches through which UMS membranes can be prepared in the future (Fig. 6) [136–183]. Biomimetic UMS membranes possess the ultrahigh permeance and spontaneous separation efficiency of cell membranes. Li and coworkers developed a biomimetic membrane by building an aquaporin Z water passageway into polyethylenimine (PEI)-crosslinked polydopamine membranes. The membranes exhibited a high NF separation performance under low pressures that were as low as 1.0 bar, significantly reducing the energy consumption required for separation [129].

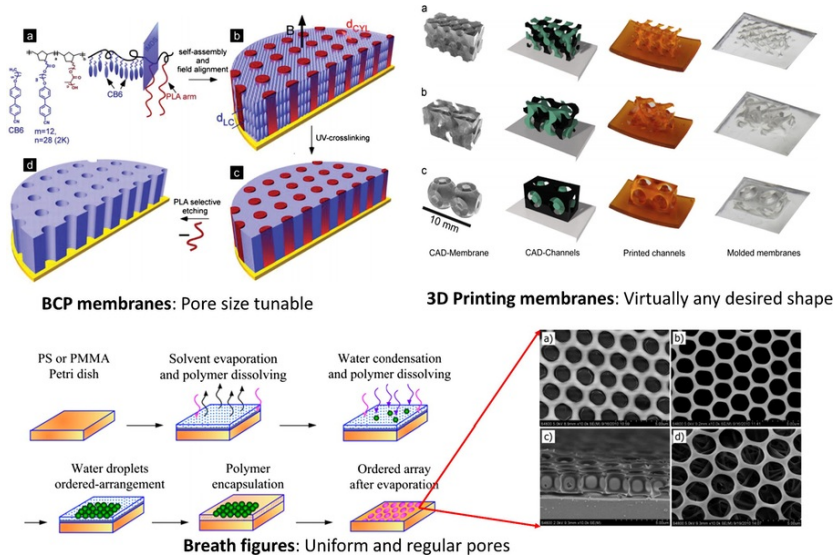

Fig. 6 (I) Typical self-assembly process of BCP membranes with ultra-uniform/regular pores: (a) Schematics of NBCB-b-NBPLA. Blue rod-shaped objects represent the cyanobiphenyl mesogens, while the blue plane is the intermaterial dividing surface (IMDS). CB6 is the free mesogen introduced into the system to accelerate the kinetics of the magnetic field alignment. (b) Magnetic alignment occurs subject to the positive anisotropy and homogeneous anchoring of the mesogens leading to the orientation of cylindrical domains along the field. (c) The system can be successively UV crosslinked yielding mechanically robust films. (d) Subsequent PLA etching from the aligned material results in a large-area nonporous membrane over mm-scale thicknesses [148]. The pores of some kinds of BCP membranes can be controlled through thermal treatment [148], pH adjustment [147] and the deposition of nanoparticles [136]. (II) The geometries of membranes fabricated by 3D printing [166]: (a) Schwarz-D, (b) Schoen-G, and (c) Schwarz-P. The designed thickness of each membrane is 1 mm, as depicted in the CAD images (far left). The independent channel sides are depicted in the middle-right column: gas channel in black and liquid channel in cyan. To prevent displacement of the separated channels in the molding process, a bottom plate is added, which is shown in white. Photos of rapidly prototyped sacrificial molds are shown in the middle-right column next to the resulting PDMS membranes after the removal of the sacrificial mold (far right). The 3D printing techniques have the potential to fabricate PDMS membranes of virtually any desired shape [166]. (III) The typical fabrication process of the "breath figure" method [158]. (IV) The typical pore structure of membranes fabricated through the "breath figure" method [159]. SEM images of a typical ordered membrane with pores, prepared from 1 mg/mL of PS-b-PDMAEMA solution in CS_2 at an air/ice interface. The airflow speed was 4 L/min. (a) Top, (b) bottom, and (c) cross-section. (d) The membrane transferred onto a piece of dense nanofiber mesh. Since the water droplet ordered arrangement induces the formation of the pores, the membranes fabricated through th breath figure method usually have uniform and regular pores, which is desirable for obtaining a high separation performance [159].

Self-assembly has also been deployed in the development of UMS membranes as this approach affords exquisite control over the formation of selective layers and membrane porosity. This process is driven by non-covalent bond interactions [137], such as hydrophobic/hydrophilic interactions [138–139], hydrogen-bonding [140], π–π interactions [141], ionic interactions~~, etc~~. Block polymers and polyelectrolytes are conventional materials for self-assembly. In the late 1990s, self-assembly was used to prepare ultrathin polymer membranes that consisted of polyelectrolytes with different charges [142–146]. Early prototypes of self-assembly membranes were usually synthesized on porous templates with thicknesses of more than 10 μm. Emerging nanomaterials such as graphene oxide and MOF nanosheets facilitate the self-assembly of free-standing and ultrathin membranes [149–153]. Graphene oxide is by far the most common material for self-assembled UMS membranes. For example, Yang and co-workers prepared free-standing graphene oxide membranes and graphene oxide/carbon nanotube hybrid membranes using an air-liquid interface by heating a graphene oxide hydrosol to 353 K [150,151]. Using the self-assembly of GO and photochemical crosslinkages, Huang et al. successfully prepared membranes consisting of a few layers of GO with adjustable molecular transportation [154]. This approach can be extended to build UMS membranes by using an elaborate self-assembling material [155]. Most recently, the shear alignment of the discotic nematic phase of graphene oxide (GO) was utilized to fabricate large scale ($13 \times 14\ cm^2$) UMS membranes by using solution casting with a lab-scale doctor blade [182]. This large-area GO membrane demonstrated a water permeance of more than $60\ L\ m^{-2}\ h^{-1}\ bar^{-1}$ for various dye solutions with high rejection (>90%) to charged and uncharged dyes with hydrated radii above 5 Å. More importantly, this work is a crucial step towards the scale-up production and commercialization of UMS membranes [182].

Other new manufacturing technologies that can be used to fabricate membranes include the "breath figure" method, 3D printing and electrophoretic gating of molecules on the membrane surface. Membranes formed using these new technologies have a high density of unblocked, uniform pores [159–183]. Unfortunately, the pores of such membranes are typically very large, rendering the resultant membranes unsuitable for UMS applications. Improvements in these technologies and the discovery of new materials are crucial for deploying these technologies for UMS membrane production, particularly 3D printing. Unlike conventional membranes, the geometry of membranes fabricated by 3D printing can be easily tailored through the manufacturing of a sacrificial mold to require higher degrees of freedom for different applications [164–166]. However, current membranes fabricated by 3D

printing are thick [164,166]. The requirement of ultrathin selective layers prevents the use of 3D printing in producing the desired UMS membranes. Another key for using 3D printing to produce UMS membranes is to develop suitable polymeric membrane materials that can be used in 3D printers.

4 UMS membrane materials

Significant effort has been devoted to developing UMS membranes using conventional polymeric materials and 2D materials (Table 1). The ultrahigh permeance of UMS membranes produced from conventional polymers is due to nanometer-thin selective layers, large pore sizes (~2 nm) and additional porosity. These polymers are chosen also because of their intrinsic high rejection rates that are similar to UF membranes. At this point, it is important to show that the ultrahigh permeances of UMS membranes are solely attributed to their physical configuration – highly porous ultrathin films. The permeabilities of these ultrathin UMS membranes are lower than $100 \times 10^{-6}\,L\,m^{-2}\,h^{-1}\,bar^{-1}$ m, comparable with their thicker analogues [24–29,57]. This infers that the ultrahigh permeance of polymeric UMS membranes is strongly dependent on membrane thickness. Interestingly, crosslinked ferritin-based UMS membranes demonstrated an ultrahigh pure water permeability of $540 \times 10^{-6}\,L\,m^{-2}\,h^{-1}\,bar^{-1}$ m, with a high rejection of dyes (protoporphyrin and direct yellow) in dilute systems. This UMS membrane had a controlled high porosity, high hydrophilicity, small pore size, and an ultrathin selective layer [26]. The ultrahigh water permeability deviates from the Hagen-Poiseuille equation. This can be ascribed to the substantially smaller membrane pore size diameter (<1 nm). Additionally, the compatibility between ferritin and water may also account for the ultrahigh permeances. Clearly, the key to yielding high quality UMS polymeric membranes is the technology responsible for fabricating ultrathin films.

Unlike polymers, 2D materials comprise rigid lamellar layers. Solvents can pass through the pores of lamellar layers, the edges of adjacent 2D materials and the nanochannels that are created through functionalization [32–56,58,62–63,74–76]. The rejection performance depends on the interval between two lamellar layers, surface charge and the total number of lamellar layers, i.e., membrane thickness. The permeances of UMS membranes based on 2D materials are less dependent on membrane thickness. This is because nanochannels for molecular transportation are easier to create in 2D materials by adjusting the lamellar layer size, pore etching, incorporating nanostrands and enlarging lamellar layer intervals [32–37,52–56,74–76]. Therefore, UMS membranes made from 2D material are usually several micrometers thick. This allows for fine adjustments in UMS membranes where permeabilities are between 100 and $2600 \times 10^{-6}\,L\,m^{-2}\,h^{-1}\,bar^{-1}m$, while the rejection performance is similar to NF (0.5–2 nm) membranes (Table 1) [32–37,52–56,74–76].

4.1 Polymeric materials for UMS membranes

Polymers are the most commonly utilized material to fabricate separation membranes. This is ascribed to their low cost and ease of scaling-up. Considering the requirement of thin selective layers (1 nm to 500 nm) in UMS membranes, polymeric materials must be robust enough to demonstrate high mechanical stability and efficient separation. Apart from crosslinked ferritin membranes, Deng et al. developed anionic charged UMS membranes by coating sulfonated polyetherketone decorated with cardo groups on a layer of copper hydroxide nanostrands above a PTFE substrate [25]. Additional water passageways within this 85 nm membrane were created by etching the nanostrands. The water flux of this membrane reached $3306\,L\,m^{-2}\,h^{-1}\,bar^{-1}$ with high rejection performance towards negatively charged solutes. Recently, Peinemann et al. developed 10 nm UMS membranes with functionalized cellulose by combining the processes of spin-coating and phase inversion, showcasing the first UMS membrane developed using conventional economical polymers. The membranes exhibited pure water permeances as high as $700\,L\,m^{-2}\,h^{-1}\,bar^{-1}$, and the selective layer was transferred onto various supports. These functionalized cellulose UMS membranes demonstrated unique selective separation performance to organic molecules with nearly 100% rejection to Reactive Black-5 and no rejection (0%) to vitamin B12 [57]. Apart from applications in aqueous solutions, polymeric UMS membranes can also be deployed in organic solvents. Nanometer-thin polymeric selective layers were used for organic solvent nanofiltration. These ultrathin membranes were supported on both crosslinked polymeric substrates and ceramic substrates [184,185]. The traditional interfacial polymerization technique was combined with the etching-coating of nanostrands to enhance solvent permeance. A 20-nm-thick polyacrylate membrane on a crosslinked polyimide substrate built by conventional interfacial polymerization techniques exhibited pure acetone permeances as high as $8.4\,L\,m^{-2}\,h^{-1}\,bar^{-1}$. This was due to an enhanced microporosity and higher interconnectivity of intermolecular network voids. The acetone permeance of this state-of-the-art polymeric UMS membrane was nearly 70 times higher than that of DuraMem DM150 membranes – a common commercial NF membrane ($0.12\,L\,m^{-2}\,h^{-1}\,bar^{-1}$) [184,185]. Most interestingly, 94 nm-thick polyamide membranes fabricated using the etching-coating process exhibited a pure acetone permeance 415 times higher than that of DuraMem DM150 membranes with a MWCO below $246\,g\,mol^{-1}$. This drastic improvement in acetone permeance and excellent selectivity was attributed to a crumpled structure, DMF activation and additional passageways created by etching sacrificial nanostrands [185].

Block copolymers (BCP) are also potentially useful for the fabrication of UMS membranes. These polymers can form a high concentration of uniform regular pores in ultrathin films [21,186–195]. Recent breakthroughs in polymer science show that the sub-10 nm pore sizes in self-assembled BCPs can be tuned with external stimuli, representing a significant advance relative to current research. Peinemann et al. prepared switchable pH-responsive BCP membranes. The pore sizes of these membranes were reduced to below 10 nm at a pH of 2 [147]. Russell et al. reported that 18 nm continuous nanopores on self-assembled polystyrene-b-poly(methyl methacrylate) (PS-b-PMMA) films could be reduced to 8 nm by swelling the PMMA microdomains [192]. Osuji et al. reported thermally switchable aligned nanopores in magnetic-field directed self-assembled BCPs [148]. However, additional studies are required to determine the water flux and size-dependent solute rejection properties of these materials. Aside from these smart strategies, techniques such as coating or the incorporation of nanomaterials may also be an effective way to reduce the

pore sizes of BCP-based membranes. The pores of poly(styrene-b-4-vinylpyridine) (PS-b-P4VP) BCP membranes were reduced by an electroless gold deposition. The pore sizes were tuned between 3 nm and 20 nm, demonstrating its potential for UMS membrane fabrication [136,194].

Inspired by PIM-based UMS membranes, another class of polymers that can be used to fabricate UMS membranes are those with a high free volume content. Examples of such polymers include PDMS, PTMSP and PMP. The main issues hampering the deployment of PDMS, PTMSP and PMP as UMS membranes are their high hydrophobicity and swelling or dissolution in non-polar solvents [196–202]. The incorporation of porous nanoparticles may enhance solvent permeance and limit the swelling of such materials, thus, promoting the possibility of the application of these materials in UMS membrane fabrication [84,196–203].

Biomimetic membranes also exhibit extremely high selectivity-permeability combinations, qualifying them as UMS membranes. Typically, these membranes are achieved by incorporating biological structures, such as aquaporin, and the construction of structures that mimic or are inspired by biological membranes [60,84,129]. Ling et al. designed an ordered multilayer membrane with nanoporous features by combining protein (silk) self-assembly and *in situ* biomineralization [60]. The thickness of these membranes were finely tailored by adjusting film formation time. These 7 µm-thick biomimetic membranes showed ultrahigh permeances of up to 1250 $L\,m^{-2}\,h^{-1}\,bar^{-1}$ and nearly 100% rejection to dyes such as Brilliant Blue G, Brilliant Blue R, Rhodamine B and Congo Red. These membranes also demonstrated high mechanical strength and were also effective for heavy metal ion removal from aqueous media. Interestingly, the cost of the biomimetic membranes is comparable with cellulose nanocrystal materials. The work of Ling et al. showcased an efficient manufacturing approach to produce biomimetic UMS membranes using peptides and proteins. This broadens the scope of UMS membrane materials while making it possible to deploy biomimetic membranes in a wide range of applications.

In summary, the development of advanced membrane manufacturing techniques and continuous focus on this field is crucial to develop UMS membranes. Many existing polymeric materials can be utilized to fabricate UMS membranes with excellent comprehensive performance, including high porosity, an ultrathin selective layer, small pore size, narrow pore size distribution, ultrahigh permeance, high rejection and high anti-fouling performance.

4.2 2D materials: an emerging UMS membrane material

Laminated 2D materials have a thickness of a few atoms, vigorous pores between different layers and high mechanical strength [32–55]. These properties differentiate them from other materials and are key requirements for fabricating UMS membranes. Intervals between the lamellar layers provide solvent passageways and play crucial roles in solute rejection [32–37,52–53,55–46,62,74–76]. The pore size, porosity and thickness of the membranes can be tailored through adjustments in the intervals between lamellar layers, size of lamellar layers and content of filtration solutions during membrane fabrication [32–37,52–53,55–56,62]. Pores can be etched in 2D materials using strong oxidants [35], enhancing membrane porosity.

Since graphene was discovered by Geim, et al. in 2004 [204], 2D materials have gained significant attention because of their electronic properties, high specific surface area and excellent mechanical strength. Liquid transportation across graphene or graphene oxide is a widely studied topic in the area of membrane science. For example, Han and coworkers developed 25–53 nm thin UMS membranes by controlling the content of chemically converted graphene. Interestingly, these membranes displayed over 99% rejection to most organic dyes and a high water permeance of 21.4 $L\,m^{-2}\,h^{-1}\,bar^{-1}$ [32]. Once single-layer graphene was deployed as the selective layer of molecular separation membranes, [40] it exhibited a salt rejection rate of nearly 100% and a water permeance of up to 25.2 $L\,m^{-2}\,h^{-1}\,bar^{-1}$ (70 $g\,m^{-2}\,s^{-1}\,atm^{-1}$) at 40 °C. Compared with graphene, graphene oxide (GO) is substantially more hydrophilic by nature, leading to a higher water permeance. GO is negatively charged, easier to disperse in water, and functionalizable for further modification; additionally, it possesses nanoscale wrinkles and structural defects. These characteristics of sub-micrometer GO sheets are attributed to the presence of oxygen-containing functional groups existing as epoxy, hydroxyl and carboxyl groups, rendering GO more suitable for USM membrane production. Qiu et al. reported the pressure-driven separation performance of thermally corrugated GO membranes with an elevated water permeance of 45 $L\,m^{-2}\,h^{-1}\,bar^{-1}$. Microscopic wrinkles in these GO membranes behaved like additional nanochannels, achieving a high permeance and selectivity [33]. Ying et al. etched pores on lamellar GO nanosheets *via* the re-oxidation of pristine GO sheets with $KMnO_4$. Interestingly, the graphene oxide sheets decreased and more mesoporous, enhancing the nanochannels between lamellar GO layers. These membranes demonstrated an excellent separation performance of 88.5% rejection for Evan's blue (EB) with a water permeance of 191 $L\,m^{-2}\,h^{-1}\,bar^{-1}$, which is nearly 3 times higher than pristine GO membranes [35]. Generating nanochanneled GO membranes through a sacrificial layer has proven to be a more efficient way to enhance the water permeance of GO-based membranes. By incorporating and etching nanostrands in the GO selective layer, additional water passageways were formed. Similarly, the intervals between monolayers of 2D materials can also be adjusted by embedding nanodots or nanotubes as mentioned above. These approaches enhanced the permeance of GO membranes by up to 492 $L\,m^{-2}\,h^{-1}$. By incorporating carbon nanodots between GO sheets, Wang et al. obtained water permeances as high as 439 $L\,m^{-2}\,h^{-1}\,bar^{-1}$ in a GO composite that rejected 96% of Rhodamine [37]. Other 2D materials were also deployed to fabricate the UMS membranes [53,54,58]. Laminar MoS_2 sheets with single atom thickness exhibited a water permeance of 245 $L\,h^{-1}\,m^{-2}\,bar^{-1}$. This is three times higher than that of pristine GO membranes with a comparable rejection performance to the Evans blue molecules (89%). High mechanical strength and good chemical stability imbue such membranes with the capability to operate under harsh conditions of continuous high pressures of up to 1.0 MPa without deforming the nanochannels [52]. Compared with the pristine GO and MoS_2 membranes, WS_2 membranes showed a substantially higher water permeance of over 700 $L\,m^{-2}\,h^{-1}\,bar^{-1}$ with a high mechanical strength and similar retention performance [53].

Other 2D material options include layered transition metal oxides (TMOs), transition metal dichalcogenides (TMDs), layered silicates and clays. These nanomaterials can be used to generate monolayered and multiple-atom

layered 2D materials [205–229]. Many challenges still exist regarding the use of 2D materials for the scale-up production of UMS membranes. The lack of low-cost 2D materials inhibit their deployment in the large-scale manufacture of UMS membranes. The dispersion and size tailoring of 2D materials prolong the membrane fabrication process, making it non-trivial to work with these materials. Most 2D material-based selective layers of UMS membranes are fabricated *via* a reduced pressure coating-etching. These selective layers are unstable when the membranes are applied in cross-flow mode [32–55]. Therefore, more efforts should be made to overcome these issues so that stable 2D-based UMS membranes can be fabricated for pilot-scale tests and potential commercialization.

4.3 Other promising emerging materials

In addition to polymeric and 2D materials, freestanding diamond such as carbon (DLC) nanosheets were developed as UMS membranes through plasma chemical vapor deposition (CVD) by Karan and coworkers [31] (Fig. 7). A 10–40 nm thin selective layer made up of carbon was successfully deposited on alumina substrates that were pre-coated with sacrificial nanostrands. When the sacrificial layer was removed by ethanol, an ultrathin, porous free-standing DLC membrane with high mechanical strength was formed. These thin DLC membranes rejected over 90% of small molecules, such as azobenzene (0.69 nm, 182.2 g mol^{-1}) and fluorescein-4-isothiocyanate (1.28 nm, 389.4 g mol^{-1}). With a similar rejection rate to commercial SRNF membranes, the solvent flux of these DLC membranes depended on the solvent viscosity, ranging from 48 L m^{-2} h^{-1} bar^{-1} to 477 L m^{-2} h^{-1} bar^{-1} [31]. The fluxes of these membranes are 600–2500 times higher than commercial SRNF membranes. In addition, Si-based and ceramic-based ultrathin selective layers are also potential structures for generating UMS membranes using the CVD technique. [20,230–232].

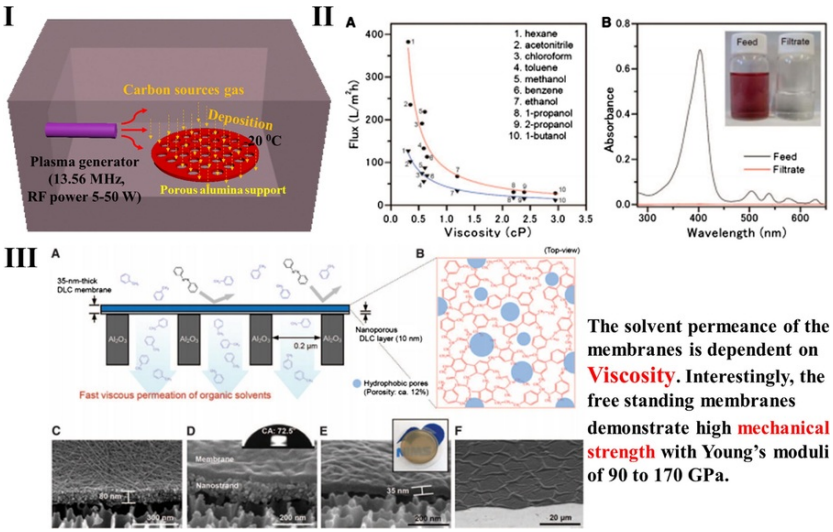

Fig. 7 The process of manufacturing diamond-like carbon membranes through CVD and their performance: (I) the fabrication process; (II) the separation performance, (A) viscosity dependent flux, (B) UV absorbance before and after filtration; and (III) the cross-section structure of diamond-like carbon membranes [31].

Porous nanoparticles also provide an efficient way to tailor pore size and shape to achieve a narrow pore size distribution that enhances permeability and selectivity [84]. Porous materials with high surface area ratios such as metal organic frameworks (MOFs) [233–238], covalent organic frameworks (COFs) [61,239–242], conjugated microporous polymers (CMPs) [243,244] and porous aromatic frameworks (PAFs) [199–202,245,246] also demonstrated great potential in the manufacturing of UMS membranes. These materials have an exceptionally high porosity, high specific surface area, uniform but tunable pore size and well-defined molecular adsorption site properties. The high specific surface area and strong absorption performance endow these materials with a high separation performance in the removal of organic solutes from water or other solvents. The intrinsic pores of these materials facilitate easier solvent transport while hindering the movement of polymer chains in mixed matrix membranes. This overcomes the physical aging in super glassy polymer membranes fabricated from PTMSP, PMP and PIMs [199–202]. This new class of nanoporous materials have garnered significant interest, particularly in membrane separation and purification applications. Attempts have been made to fabricate mixed matrix membranes containing MOF additives [59,247–254]. The small pore size of ZIF and the thick selective layers lead to membranes with poor cut-off properties. Hence, hydrostable nanoporous materials with suitable pore sizes must be deployed in ultrathin polymeric films to fully optimize the advantages of these materials in UMS membranes. Zhang et al. constructed MOF-hybrid membranes through the coordination-driven *in situ* self-assembly of poly(sodium 4-styrenesulfonate) (PSS) and ZIF-8 [29]. They reported that the self-assembling conditions of MOFs influenced the membrane separation performance. The particle size of ZIF-8 was reduced by increasing the concentration of ZIF-8 precursors, such as $Zn(NO_3)_2$. This enhanced methyl blue (MB)

rejection while decreasing water permeance. When the concentration of $Zn(NO_3)_2$ was 0.05 mol L^{-1}, these ZIF-8/PSS membranes demonstrated water permeances as high as 26.5 L m^{-2} h^{-1} bar^{-1} with a 98.6% MB removal rate [59]. In addition to ZIF-8, UiO-66, a hydro- and chemical-stable MOF is also preferred for UMS membranes [255–257]. The post-synthetic exchange of metal ions from Zr to Ti or Hf can tune the pore size of UiO-66 to suit various applications [258,259]. Moreover, the pore size and dispersion of UiO-66 in polymer matrices can also be tailored with different ligands [257], functionalization [260,261] and grafting water-soluble polymers [262].

Self-supporting membranes derived from these nanoporous materials are ideal UMS membranes [61,84]. The ultrahigh porosity and narrow pore size distribution of these materials can yield ultrapermeable membranes that are highly selective. However, these membranes are often plagued by poor mechanical strength and intrinsic or external defects [84]. Key to producing UMS membranes using nanoporous materials is to minimize defects [84]. Kandambeth and coauthors developed a 290 μm self-supporting COF membrane [61] that exhibited 99% rejection to vitamin B12 (MW = 1344 Da) and 81% rejection to tetracycline (MW = 444 Da), an antimicrobial drug. With large amounts of intrinsic pores, this COF membrane demonstrated an acetonitrile permeance of 180 L m^{-2} h^{-1} bar^{-1} (a permeability of 52200 L m^{-2} h^{-1} bar^{-1} m). This is twice as large as those of existing polyamide-based NF membranes [61]. Because of well-organized, ordered pores within the COF structure and ultrahigh chemical and structural stabilities, the COF membranes demonstrate a high permeability to organic solvents and high selectivity. This offers a solution to address both environmental problems and issues in pharmaceutical production [61].

Liquid crystalline materials, especially liquid crystal polymers, can yield membranes with high fluxes [263–266]. Liquid crystal polymer chains can be homeotropically aligned in a direction that is parallel to molecular transport. This unique property of liquid crystal polymers can also be used to orient nanotubes in the direction of molecular transport across the membrane. The approach of using membranes fabricated from liquid crystals has so far been demonstrated on RO membranes for desalination only [263–266]. The rejection of these membranes is high; however, their permeances are insufficient to process the large quantities of feed mixtures in industry. The main issues with these membranes include a thick selective layer and a lack of nanochannels in the membranes for water transport.

The rapid development of nanotechnology and advanced membrane fabrication methodologies coupled with exciting advances in materials development open up a plethora of combinations and opportunities to fabricate UMS membranes with excellent properties. However, it must be kept in mind that each material inherently has unique properties and its own set of problems. Based on membrane properties such as permeance, rejection, mechanical strength, membrane stability and cost, the possibility of using various cutting-edge materials to scale-up the production of UMS membranes is summarized and evaluated in Table 2. For instance, the high pore density and uniform pore size distribution of BCP membranes lead to ultrahigh permeability [21,186–195]. However, it is hard to tailor the mean effective pore size below 5 nm [21,186–195], and the significant cost of BCPs hampers the commercialization potential of these membranes. Therefore, the technology-readiness level of BCP-based UMS membranes is believed to be low. Compared with BCPs, graphene or graphene oxide appears to be more feasible for use in UMS membranes. This is because the nanochannels between GO layers for solvent transport are easier to create and manipulate. This can be achieved by adjusting inter-lamellar layer distance, pore etching, incorporating nanostrands and enlarging lamellar layer intervals [32–37,52–53,55–56,62]. Thermal reduction can also be deployed to obtain robust carbonaceous composite GO-based membranes containing graphene quantum dots (GQDs) and thermally reduced graphene oxide (TRG) (GQDs-TRG). Similar to other GO membranes with nanochannels, the GQDs-TRG membranes demonstrated an excellent long-term continuous separation performance in cross-flow mode with a water permeance of 2000 ± 70 L m^{-2} h^{-1} bar^{-1} and high rejection to EB (96 ± 0.2%). More importantly, these GQDs-TRG selective layers were stable even after 10 min of strong sonication, promoting the possible application of these UMS membranes in harsh operating conditions. The high cost of GO membranes coupled with complicated processes to produce stable graphene oxides continue to hamper their applications. Hence, the technology-readiness level and potential of graphene/graphene oxide-based materials to be manufactured as UMS membranes is marked as medium.

Table 2 Materials that are possible to be developed as selective layer of UMS membranes.

Materials type		Fabrication method	Advantages	Technology readiness level	Typical references
Polymers	Porous polymers (NF)	Evaporating-coating	High selectivity & high permeance to heptane	Medium	[17]
	Polymers with nanochannels etched by nanostrands (UF)	Filtration-coating	Ultra high permeability	Medium	[25,27–29]
	Polymers with porous additives (COFs, MOFs, PAFs) (NF)	Coating/Assembly	High Selectivity	Medium	[59,201–203,251–252]
	BCPs (UF)	Breath-figure	Uniform pores with high permeable properties	Far	[21,147,148]
	Biomimetic polymer or polymers with biomimetic additives (NF)	Filtration-coating-crosslinking	Ultrahigh permeability and high selectivity	Near	[26,60,129]
	Other polymers (UF/NF)	Spin-coating	High permeability	Medium	[57,166]

Free-standing COFs or MOFs membranes (NF)		Evaporating	High permeability and selectivity	Medium	[61,254]
2D materials	Graphene/Graphene oxide (NF)	Filtration-coating	High selectivity	Far	[32,35]
	Graphene/Graphene oxide with nanochannels (NF)	Filtration-coating	High selectivity and high permeability	Medium	[36,37,55,62]
	Other 2D materials (NF) with nanochannels	Filtration-coating	High selectivity and high permeability	Medium	[52,53,58]
Other materials	Carbon or Si-based materials (NF)	CVD/3D printing	High selectivity and high permeability	Medium	[31,169,181]
	Liquid crystal materials	Transcription method	High selectivity	Far	[263–266]
	Janus membranes	Surface modifications	High permeability	Far	[275,276]

5 Outlook—challenges overhead

The lack of advances in material sciences and the development of fabrication techniques are the basic and most important challenges that impede the progression of UMS membranes. In addition, the exploration of new applications especially for dilute system separations can accelerate the progression of UMS membranes. Currently, only a few types of polymers and 2D materials are suitable for the fabrication of UMS membranes using the coating-etching method or phase inversion-coating method. Biomimetic materials, block-copolymers, liquid crystals and porous frameworks, such as MOFs, COFs, and PAFs, are alternative building blocks for UMS membranes [184–193,230–263]. Unfortunately, the costs of these materials remain high, inhibiting the scale-up production of low-cost UMS membranes. Cutting-edge technologies such as 3D printing, “breath figures” and the electrophoretic gating of molecules at membrane surfaces may provide more choices to control pore formation in UMS membranes [143–183].

A good theoretical separation model is required to predict mass transfer across membranes and provide guidance to designing UMS membranes. A lack of suitable characterization techniques to precisely measure pore size distribution, porosity and membrane thickness curtails the design of UMS membranes and the quantitative analysis of mass transfer across UMS membranes. According to standard fluid dynamics, the Hagen-Poiseuille equation is useful for predicting the flux of UMS membranes and analyze the crucial factors that affect the flux. However, it is extremely difficult to find a basic theory that predicts a flux value that is consistent with the experimental results because fluid flow through a nanosized pore is an extremely complicated system. In addition to the conformation of pores, the fluid should be a laminar flow through cylindrical pores in an incompressible and Newtonian mode according to the Hagen-Poiseuille law. If the liquid velocity through the pores or the diameter of the pores exceeds a threshold, laminar flow becomes turbulent flow. This may occur in UMS membranes because of their unique pore size and ultrafast fluid flux. Therefore, advanced fluid dynamics should be developed to consider the unique properties of UMS membranes, in which molecular simulation may play a key role [267–271]. There remains plenty of challenges to overcome to clarify the reasons behind ultrafast mass transfer across UMS membranes, which is the key to providing guidance to the design of advanced UMS membranes.

Currently, the main research thrusts in the field of UMS membranes are focused on yielding ultrafast flux and high rejection rates of UMS membranes. Taking practical applications of UMS membranes into consideration, one should also focus on the impacts of module design, concentration polarization and other properties, such as the anti-fouling performance and mechanical strength. Most works have utilized the dead-end test, precluding the effects of concentration polarization and membrane fouling. More results obtained from cross-flow tests should be reported to gauge the feasibility of using UMS membranes in turbulent operating conditions. At the same time, the compatibility between ultra-thin selective layers and supports, and mechanical stability of UMS membrane will be challenged by the shear strength during the cross-flow mode. The design of the membrane module also affects the separation performance of the whole membrane system. This in turn determines the solution flow type in the module. A major advantage of UMS membranes is the ability to reduce the required membrane surface area in the module. This results in smaller membrane modules and considerable capital costs. In addition to the membrane surface area, a reasonable arrangement of the flow channel is conducive to promote the mass transfer process across the membrane. In such circumstances, module design is extremely important to maximize the benefits of deploying UMS membranes. In fact, this is even more important than developing new UMS membranes [78,82–84]. However, there is no corresponding research focusing on the design of a membrane module for UMS membranes. Therefore, more efforts should be devoted to developing new modules that can accelerate the deployment of UMS membranes for large-scale applications.

Despite the many remaining challenges, emerging UMS membranes offer a promising solution for environmental remediation and resolving the energy shortage by their ability to replace traditional separation processes for removing/recycling the organic active molecules from dilute solutions. With an ultrathin, dense selective layer, UMS membranes can separate nanosized molecules, such as dyes, from water or solvents with an ultrafast flux that is several times higher than that of existing commercial NF/UF membranes. Driven by potential profits from reduced energy consumption and a low-efficiency separation technique to separate active molecules, great advances in this field can be imagined in the near future. In addition to the current expected use of UMS membranes in the petrochemical, food, pharmaceutical, and water treatment industries, these membranes can also be exploited in the burgeoning fields of biological and medical industries. A new membrane module design should be continuously explored, such as the integration of the selective layer into smart Janus membranes with an asymmetric ion structure (Fig. 8) [272–276]. Furthermore, unique applications of UMS membranes can be explored in microchemical reactors and medical one-way valves.

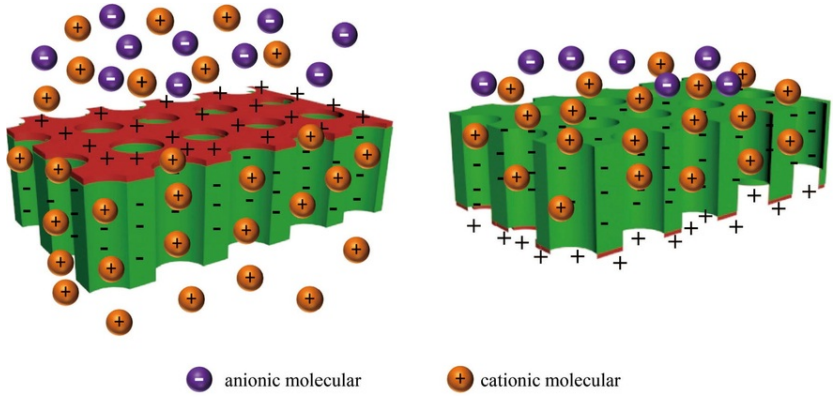

Fig. 8 The potential novel Janus membranes with asymmetric ion structure for molecular separation.

Acknowledgements

This work was supported by National Natural Science Foundation of China (21676063, U1462103), State Key Laboratory of Urban Water Resource and Environment (Harbin Institute Technology) (No. 2017DX07), and HIT Environment and Ecology Innovation Special Funds (HSCJ201619).

References

[1] M. Elimelech and W.A. Phillip, The future of seawater desalination: energy, technology, and the environment, *Science* **333** (6043), 2011, 712–717.

[2] M.A. Shannon, P.W. Bohn, M. Elimelech, J.G. Georgiadis, B.J. Mariñas and A.M. Mayes, Science and technology for water purification in the coming decades, *Nature* **452**, 2008, 301–310.

[3] W.J. Koros and C. Zhang, Materials for next-generation molecularly selective synthetic membranes, *Nat Mater* **16**, 2017, 289–297.

[4] R.P. Lively and D.S. Sholl, From water to organics in membrane separations, *Nat Mater* **16**, 2017, 276–279.

[5] Y. Xiao, B.T. Low, S.S. Hosseini, T.S. Chung and D.R. Paul, The strategies of molecular architecture and modification of polyimide-based membranes for CO_2 removal from natural gas—a review, *Prog Polym Sci* **34**, 2009, 561–580.

[6] L.Y. Jiang, Y. Wang, T.S. Chung, X.Y. Qiao and J.Y. Lai, Polyimides membranes for pervaporation and biofuels separation, *Prog Polym Sci* **34**, 2009, 1135–1160.

[7] P. Vandezande, L.E.M. Gevers and I.F.J. Vankelecom, Solvent resistant nanofiltration separating on a molecular level, *Chem Soc Rev* **37**, 2008, 365–405.

[8] P. Marchetti, M.F. Jimenez Solomon, G. Szekely and A.G. Livingston, Molecular separation with organic solvent nanofiltration: a critical review, *Chem Rev* **114**, 2014, 10735–10806.

[9] G. Szekely, M.F. Jimenez-Solomon, P. Marchetti, J.F. Kim and A.G. Livingston, Sustainability assessment of organic solvent nanofiltration: from fabrication to application, *Green Chem* **16**, 2014, 4440–4473.

[10] L.S. White, Development of large-scale applications in organic solvent nanofiltration and pervaporation for chemical and refining processes, *J Membr Sci* **286**, 2006, 26–35.

[11] X.Q. Cheng, Y.L. Zhang, Z.X. Wang, Z.H. Guo, Y.P. Bai and L. Shao, Recent advances in polymeric solvent-resistant nanofiltration membranes, *Adv Polym Technol* **33**, 2014, E1–E4.

[12] Z.X. Wang, C.H. Lau, N.Q. Zhang, Y.P. Bai and L. Shao, Mussel-inspired tailoring of membrane wettability for harsh water treatment, *J Mater Chem A* **3**, 2015, 2650–2657.

[13] Y.Q. Zhang, X.B. Yang, Z.X. Wang, J. Long and L. Shao, Designing multifunctional 3D magnetic foam for effective insoluble oil separation and rapid selective dye removal for use in wastewater remediation, *J Mater Chem A* **5**, 2017, 7316–7325.

[14] X. Jiang, S.W. Li and L. Shao, Pushing CO_2-philic membrane performance to the limit by designing semi-interpenetrating networks for sustainable CO_2 separations, *Energy Environ Sci* **10**, 2017, 1339–1344.

[15] X.B. Yang, X. Jiang, Y.D. Huang, Z.H. Guo and L. Shao, Building nanoporous metal-organic frameworks “armour” on fibers for high-performance composite materials, *ACS Appl Mater Interf* **9**, 2017, 5590–5599.

[16] Y.C. Xu, Y.P. Tang, L.F. Liu, Z.H. Guo and L. Shao, Nanocomposite organic solvent nanofiltration membranes by a highly-efficient mussel-inspired co-deposition strategy, *J Membr Sci* **526**, 2017, 32–42.

[17] Y.C. Xu, Z.X. Wang, X.Q. Cheng, Y.C. Xiao and L. Shao, Positively charged nanofiltration membranes via economically mussel-substance-simulated co-deposition for textile wastewater treatment, *Chem Eng J* **303**, 2016, 555–564.

[18] F.P. Cuperus and C.A. Smolders, Characterization of UF membranes: membrane characteristics and characterization techniques, *Adv Colloid Interf* **34**, 1991, 135–173.

[19] X. Feng, S. Nejati, M.G. Cowan, M.E. Tousley, B.R. Wiesenauer, R.D. Noble, et al., Thin polymer films with continuous vertically aligned 1 nm pores fabricated by soft confinement, *ACS Nano* **10**, 2016, 150–158.

[20] C.C. Striemer, T.R. Gaborski, J.L. McGrath and P.M. Fauchet, Charge-and size-based separation of macromolecules using ultrathin silicon membranes, *Nature* **445**, 2007, 749–753.

[21] Z. Wang, X. Yao and Y. Wang, Swelling-induced mesoporous block copolymer membranes with intrinsically active surfaces for size-selective separation, *J Mater Chem* **22**, 2012, 20542–20548.

[22] X. Wang, D. Fang, K. Yoon, B.S. Hsiao and B. Chu, High performance ultrafiltration composite membranes based on poly (vinyl alcohol) hydrogel coating on crosslinked nanofibrous poly (vinyl alcohol) scaffold, *J Membr Sci* **278**, 2006, 261–268.

[23] M. Sahimi, Flow and transport in porous media and fractured rock, 1995, VCH.

[24] P. Gorgojo, S. Karan, H.C. Wong, M.F. Jimenez-Solomon, J.T. Cabral and A.G. Livingston, Ultrathin polymer films with intrinsic microporosity: anomalous solvent permeation and high flux membranes, *Adv Func Mater* **24**, 2014, 4729–4737.

[25] C. Deng, Q.G. Zhang, G.L. Han, Y. Gong, A.M. Zhu and Q.L. Liu, Ultrathin self-assembled anionic polymer membranes for superfast size-selective separation, *Nanoscale* **5**, 2013, 11028–11034.

[26] X. Peng, J. Jin, Y. Nakamura, T. Ohno and I. Ichinose, Ultrafast permeation of water through protein-based membranes, *Nat Nanotechnol* **4**, 2009, 353–357.

[27] Q. Zhang, S. Ghosh, S. Samitsu, X. Peng and I. Ichinose, Ultrathin freestanding nanoporous membranes prepared from polystyrene nanoparticles, *J Mater Chem* **21**, 2011, 1684–1688.

[28] L. Shi, Q. Yu, H. Huang, Y. Mao, J. Lei, Z. Ye, et al., Superior separation performance of ultrathin gelatin films, *J Mater Chem A* **1**, 2013, 1899–1906.

[29] Q. Wang, S. Samitsu and I. Ichinose, Ultrafiltration membranes composed of highly cross-linked cationic polymer gel: the network structure and superior separation performance, *Adv Mater* **23**, 2011, 2004–2008.

[30] G. Fu, Z. Su, X. Jiang and J. Yin, Photo-crosslinked nanofibers of poly (ether amine)(PEA) for the ultrafast separation of dyes through molecular filtration, *Polym Chem* **5**, 2014, 2027–2034.

[31] S. Karan, S. Samitsu, X. Peng, K. Kurashima and I. Ichinose, Ultrafast viscous permeation of organic solvents through diamond-like carbon nanosheets, *Science* **335**, 2012, 444–447.

[32] Y. Han, Z. Xu and C. Gao, Ultrathin graphene nanofiltration membrane for water purification, *Adv Func Mater* **23**, 2013, 3693–3700.

[33] L. Qiu, X. Zhang, W. Yang, Y. Wang, G.P. Simon and D. Li, Controllable corrugation of chemically converted graphene sheets in water and potential application for nanofiltration, *Chem Commun* **47**, 2011, 5810–5812.

[34] H. Huang, Y. Mao, Y. Ying, Y. Liu, L. Sun and X. Peng, Salt concentration, pH and pressure controlled separation of small molecules through lamellar graphene oxide membranes, *Chem Commun* **49**, 2013, 5963–5965.

[35] Y. Ying, L. Sun, Q. Wang, Z. Fan and X. Peng, In-plane mesoporous graphene oxide nanosheet assembled membranes for molecular separation, *RSC Adv* **4**, 2014, 21425–21428.

[36] H. Huang, Z. Song, N. Wei, L. Shi, Y. Mao, Y. Ying, et al., Ultrafast viscous water flow through nanostrand-channelled graphene oxide membranes, *Nat Commun* **4**, 2013, 2979.

[37] W. Wang, E. Eftekhari, G. Zhu, X. Zhang, Z. Yan and Q. Li, Graphene oxide membranes with tunable permeance due to embedded carbon dots, *Chem Commun* **50**, 2014, 13089–13092.

[38] J. Luo, J. Kim and J. Huang, Material processing of chemically modified graphene: some challenges and solutions, *Acc Chem Res* **46**, 2013, 2225–2234.

[39] W. Yuan, J. Chen and G. Shi, Nanoporous graphene materials, *Mater Today* **17**, 2014, 77–85.

[40] S.P. Surwade, S.N. Smirnov, I.V. Vlassiouk, R.R. Unocic, G.M. Veith, S. Dai, et al., Water desalination using nanoporous single-layer graphene, *Nat Nanotechnol* **10**, 2015, 459–464.

[41] H. Liu, H. Wang and X. Zhang, Facile fabrication of freestanding ultrathin reduced graphene oxide membranes for water purification, *Adv Mater* **27**, 2015, 249–254.

[42] B. Mi, Graphene oxide membranes for ionic and molecular sieving, *Science* **343**, 2014, 740–742.

[43] S.C. O'Hern, M.S. Boutilier, J.C. Idrobo, Y. Song, J. Kong, T. Laoui, et al., Selective ionic transport through tunable subnanometer pores in single-layer graphene membranes, *Nano Lett* **14**, 2014, 1234–1241.

[44] Y.M. Lee, B. Jung, Y.H. Kim, A.R. Park, S. Han, W.S. Choe, et al., Nanomesh-structured ultrathin membranes harnessing the unidirectional alignment of viruses on a graphene-oxide film, *Adv Mater* **26**, 2014, 3899–3904

[45] R.R. Nair, H.A. Wu, P.N. Jayaram, I.V. Grigorieva and A.K. Geim, Unimpeded permeation of water through helium-leak–tight graphene-based membranes, *Science* **335**, 2012, 442–444.

[46] R.K. Joshi, P. Carbone, F.C. Wang, V.G. Kravets, Y. Su, I.V. Grigorieva, et al., Precise and ultrafast molecular sieving through graphene oxide membranes, *Science* **343**, 2014, 752–754.

[47] C.N. Yeh, K. Raidongia, J. Shao, Q.H. Yang and J. Huang, On the origin of the stability of graphene oxide membranes in water, *Nat Chem* **7**, 2015, 166–170.

[48] P. Sun, M. Zhu, K. Wang, M. Zhong, J. Wei, D. Wu, et al., Selective ion penetration of graphene oxide membranes, *ACS Nano* **7**, 2012, 428–437.

[49] N. Wei, X. Peng and Z. Xu, Understanding water permeation in graphene oxide membranes, *ACS Appl Mater Interf* **6**, 2014, 5877–5883.

[50] W. Xiong, J.Z. Liu, M. Ma, Z. Xu, J. Sheridan and Q. Zheng, Strain engineering water transport in graphene nanochannels, *Phys Rev E* **84**, 2011, 056329.

[51] H. Huang, Y. Ying and X. Peng, Graphene oxide nanosheet: an emerging star material for novel separation membranes, *J Mater Chem A* **2**, 2014, 13772–13782.

[52] L. Sun, H. Huang and X. Peng, Laminar MoS_2 membranes for molecule separation, *Chem Commun* **49**, 2013, 10718–10720.

[53] L. Sun, Y. Ying, H. Huang, Z. Song, Y. Mao, Z. Xu, et al., Ultrafast molecule separation through layered WS_2 nanosheet membranes, *ACS Nano* **8**, 2014, 6304–6311.

[54] K. Raidongia and J. Huang, Nanofluidic ion transport through reconstructed layered materials, *J Am Chem Soc* **134**, 2012, 16528–16531.

[55] S.J. Gao, H. Qin, P. Liu and J. Jin, SWCNT-intercalated GO ultrathin films for ultrafast separation of molecules, *J Mater Chem A* **3**, 2015, 6649–6654.

[56] L. Huang, J. Chen, T. Gao, M. Zhang, Y. Li, L. Dai, et al., Reduced graphene oxide membranes for ultrafast organic solvent nanofiltration, *Adv Mater* **28**, 2016, 8669–8674.

[57] T. Puspasari, H. Yu and K.V. Peinemann, Charge-and size-selective molecular separation using ultrathin cellulose membranes, *Chemsuschem* **9**, 2016, 2908–2911.

[58] Y. Qu, Q.G. Zhang, F. Soyekwo, R.S. Gao, R.X. Lv, C.X. Lin, et al., Nickel hydroxide nanosheet membranes with fast water and organics transport for molecular separation, *Nanoscale* **8**, 2016, 18428–18435.

[59] R. Zhang, S. Ji, N. Wang, L. Wang, G. Zhang and J.R. Li, Coordination-driven in situ self-assembly strategy for the preparation of metal-organic framework hybrid membranes, *Angew Chem Int Ed* **53**, 2014, 9775–9779.

[60] S. Ling, Z. Qin, W. Huang, S. Cao, D.L. Kaplan and M. Buehler, Design and function of biomimetic multilayer water purification membranes, *Sci Adv* **3**, 2017, e1601939, https://doi.org/10.1126/sciadv.1601939.

[61] S. Kandambeth, B.P. Biswal, H.D. Chaudhari, K.C. Rout, H. Kunjattu, S. Mitra, et al., Selective molecular sieving in self-standing porous Covalent-Organic-Framework membranes, *Adv Mater* **29**, 2017, 1603945.

[62] Y. Ying, P. He, M. Wei, G. Ding and X. Peng, Robust GQDs modified thermally reduced graphene oxide membranes for ultrafast and long-term purification of dye-wasted water, *Adv Mater Interf* 2017, 1700209, https://doi.org/10.1002/admi.201700209.

[63] Y. Qin, Y. Hu, S. Koehler, L. Cai, J. Wen, X. Tan, et al., Ultrafast nanofiltration through large-area single-layered graphene membranes, *ACS Appl Mater Interf* **9**, 2017, 9239–9244.

[64] X.J. Yang, A.G. Livingston and L.F. Dos Santos, Experimental observations of nanofiltration with organic solvents, *J Membr Sci* **190**, 2001, 45–55.

[65] B. Van der Bruggen, J. Geens and C. Vandecasteele, Influence of organic solvents on the performance of polymeric nanofiltration membranes, *Sep Sci Technol* **37**, 2002, 783–797.

[66] Y.S. Toh, X.X. Loh, K. Li, A. Bismarck and A.G. Livingston, In search of a standard method for the characterisation of organic solvent nanofiltration membranes, *J Membr Sci* **291**, 2007, 120–125.

[67] L. Hesse, J. Mićović, P. Schmidt, A. Górak and G. Sadowski, Modelling of organic-solvent flux through a polyimide membrane, *J Membr Sci* **428**, 2013, 554–561.

[68] S. Darvishmanesh, T. Robberecht, P. Luis, J. Degrève and B. Van der Bruggen, Performance of nanofiltration membranes for solvent purification in the oil industry, *J Am Oil Chem Soc* **88**, 2011, 1255–1261.

[69] D. Ormerod, B. Sledsens, G. Vercammen, D. Van Gool, T. Linsen, A. Buekenhoudt, et al., Demonstration of purification of a pharmaceutical intermediate via organic solvent nanofiltration in the presence of acid, *Sep Purif Technol* **115**, 2013, 158–162.

[70] B. Tylkowski, B. Trusheva, V. Bankova, M. Giamberini, G. Peev and A. Nikolova, Extraction of biologically active compounds from propolis and concentration of extract by nanofiltration, *J Membr Sci* **348**, 2010, 124–130.

[71] G. Székely, J. Bandarra, W. Heggie, B. Sellergren and F.C. Ferreira, Organic solvent nanofiltration: a platform for removal of genotoxins from active pharmaceutical ingredients, *J Membr Sci* **381**, 2011, 21–33.

[72] J. Tanninen, S. Platt, A. Weis and M. Nyström, Long-term acid resistance and selectivity of NF membranes in very acidic conditions, *J Membr Sci* **240**, 2004, 11–18.

[73] F. Zhou, C. Wang and J. Wei, Separation of acetic acid from monosaccharides by NF and RO membranes: performance comparison, *J Membr Sci* **429**, 2013, 243–251.

[74] Y. Ying, Y. Yang, W. Ying and X. Peng, Two-dimensional materials for novel liquid separation membranes, *Nanotechnology* **27**, 2016, 332001.

[75] Z. Zheng, R. Grünker and X. Feng, Synthetic two-dimensional materials: a new paradigm of membranes for ultimate separation, *Adv Mater* **28**, 2016, 6529–6545.

[76] G. Liu, W. Jin and N. Xu, Two-dimensional-material membranes: a new family of high-performance separation membranes, *Angew Chem Int Ed* **55**, 2016, 13384–13397.

[77] S. Dervin, D.D. Dionysiou and S.C. Pillai, 2D nanostructures for water purification: graphene and beyond, *Nanoscale* **8**, 2016, 15115–15131.

[78] B. Shi, P. Marchetti, D. Peshev, S. Zhang and A.G. Livingston, Will ultra-high permeance membranes lead to ultra-efficient processes? Challenges for molecular separations in liquid systems, *J Membr Sci* **525**, 2017, 35–47.

[79] S. Sundaramoorthy, G. Srinivasan and D.V.R. Murthy, An analytical model for spiral wound reverse osmosis membrane modules: Part I—model development and parameter estimation, *Desalination* **280**, 2011, 403–411

[80] M.L. Crowder and C.H. Gooding, Spiral wound, hollow fiber membrane modules: a new approach to higher mass transfer efficiency, *J Membr Sci* **137**, 1997, 17–29.

[81] B. Shi, D. Peshev, P. Marchetti, S. Zhang and A.G. Livingston, Multi-scale modelling of OSN batch concentration with spiral-wound membrane modules using OSN Designer, *Chem Eng Res Des* **109**, 2016, 385–396.

[82] D. Cohen-Tanugi, R.K. McGovern, S.H. Dave, J.H. Lienhard and J.C. Grossman, Quantifying the potential of ultra-permeable membranes for water desalination, *Energy Environ Sci* **7**, 2014, 1134–1141.

[83] A. Deshmukh, N.Y. Yip, S. Lin and M. Elimelech, Desalination by forward osmosis: identifying performance limiting parameters through module scale modelling, *J Membr Sci* **491**, 2015, 159–167.

[84] H.B. Park, J. Kamcev, L.M. Robeson, M. Elimelech and B.D. Freeman, Maximizing the right stuff: the trade-off between membrane permeability and selectivity, *Science* **356**, 2017, eaab0530;
A. Yunessnia lehi, A. Akbari and Z. Ghaedamini haruni, Preparation of novel thin-film composite nanofiltration membranes for separation of amoxicillin, *J Nanostruct* **4**, 2014, 199–210.

[85] K.Y. Wang and T.S. Chung, Polybenzimidazole nanofiltration hollow fiber for cephalexin separation, *AIChE J* **52**, 2006, 1363–1377.

[86] M. Homayoonfal and M.R. Mehrnia, Amoxicillin separation from pharmaceutical solution by pH sensitive nanofiltration membranes, *Sep Purif Technol* **130**, 2014, 74–83.

[87] G. Székely, I.B. Valtcheva, J.F. Kim and A.G. Livingston, Molecularly imprinted organic solvent nanofiltration membranes–revealing molecular recognition and solute rejection behavior, *React Funct Polym* **86**, 2015, 215–224.

[88] D. Rana, B. Scheier, R.M. Narbaitz, T. Matsuura, S. Tabe, S.Y. Jasim, et al., Comparison of cellulose acetate (CA) membrane and novel CA membranes containing surface modifying macromolecules to remove pharmaceutical and personal care product micropollutants from drinking water, *J Membr Sci* **409**, 2012, 346–354.

[89] M. Priske, M. Lazar, C. Schnitzer and G. Baumgarten, Recent applications of organic solvent nanofiltration, *Chem Ing Tec* **88**, 2016, 39–49.

[90] R.W. Baker, Membrane technology and applications, 2nd ed., 2004, John Wiley & Sons Ltd.; Chichester.

[91] H. Lin, E. Van Wagner, B.D. Freeman, L.G. Toy and R.P. Gupta, Plasticization-enhanced hydrogen purification using polymeric membranes, *Science* **311**, 2006, 639–642.

[92] P. Dietz, P.K. Hansma, O. Inacker, H.D. Lehmann and K.H. Herrmann, Surface pore structures of micro-and ultrafiltration membranes imaged with the atomic force microscope, *J Membr Sci* **65**, 1992, 101–111.

[93] D. Bhanushali, S. Kloos and D. Bhattacharyya, Solute transport in solvent-resistant nanofiltration membranes for non-aqueous systems: experimental results and the role of solute–solvent coupling, *J Membr Sci* **208**, 2002, 343–359.

[94] J. Gilron, N. Gara and O. Kedem, Experimental analysis of negative salt rejection in nanofiltration membranes, *J Membr Sci* **185**, 2001, 223–236.

[95] P. Silva and A.G. Livingston, Effect of solute concentration and mass transfer limitations on transport in organic solvent nanofiltration—partially rejected solute, *J Membr Sci* **280**, 2006, 889–898.

[96] P. Silva, S. Han and A.G. Livingston, Solvent transport in organic solvent nanofiltration membranes, *J Membr Sci* **262**, 2005, 49–59.

[97] Y.H. See-Toh, F.C. Ferreira and A.G. Livingston, The influence of membrane formation parameters on the functional performance of organic solvent nanofiltration membranes, *J Membr Sci* **299**, 2007, 236–250.

[98] H.K. Lonsdale, U. Merten and R.L. Riley, Transport properties of cellulose acetate osmotic membranes, *J Appl Polym Sci* **9**, 1965, 1341–1362.

[99] J.G. Wijmans and R.W. Baker, The solution-diffusion model: a review, *J Membr Sci* **107**, 1995, 1–21.

[100] W.R. Bowen and J.S. Welfoot, Modelling of membrane nanofiltration—pore size distribution effects, *Chem Eng Sci* **57**, 2002, 1393–1407.

[101] S.S. Sablani, M.F.A. Goosen, R. Al-Belushi and M. Wilf, Concentration polarization in ultrafiltration and reverse osmosis: a critical review, *Desalination* **141**, 2002, 269–289.

[102] A. Seidel and M. Elimelech, Coupling between chemical and physical interactions in natural organic matter (NOM) fouling of nanofiltration membranes: implications for fouling control, *J Membr Sci* **203**, 2002, 45–255.

[103] A.L. Zydney and C.K. Colton, A concentration polarization model for the filtrate flux in cross-flow microfiltration of particulate suspensions, *Chem Eng Commun* **47**, 1986, 1–21.

[104] R. Bian, K. Yamamoto and Y. Watanabe, The effect of shear rate on controlling the concentration polarization and membrane fouling, *Desalination* **131**, 2000, 225–236.

[105] M. Kattula, K. Ponnuru, L. Zhu, W. Jia, H. Lin and E.P. Furlani, Designing ultrathin film composite membranes: the impact of a gutter layer, *Sci Rep* **5**, 2015, 15016.

[106] Y.C. Xu, X.Q. Cheng, J. Long and L. Shao, A novel monoamine modification strategy toward high-performance organic solvent nanofiltration (OSN) membrane for sustainable molecular separations, *J Membr Sci* **497**, 2016, 77–89.

[107] Y.P. Tang, J.X. Chan, T.S. Chung, M. Weber, C. Staudt and C. Maletzko, Simultaneously covalent and ionic bridging towards antifouling of GO-imbedded nanocomposite hollow fiber membranes, *J Mater Chem A* **3**, 2015 10573–10584.

[108] B. Bolto, M. Hoang and Z. Xie, A review of membrane selection for the dehydration of aqueous ethanol by pervaporation, *Chem Eng Process* **50**, 2011, 227–235.

[109] B. Bolto, T. Tran, M. Hoang and Z. Xie, Crosslinked poly (vinyl alcohol) membranes, *Prog Polym Sci* **34**, 2009, 969–981.

[110] S. Hermans, H. Mariën, C. Van Goethem and I.F. Vankelecom, Recent developments in thin film (nano) composite membranes for solvent resistant nanofiltration, *Curr Opin Chem Eng* **8**, 2015, 45–54.

[111] L. Shao, X.Q. Cheng, Y. Liu, S. Quan, J. Ma, S.Z. Zhao, et al., Newly developed nanofiltration (NF) composite membranes by interfacial polymerization for Safranin O and Aniline blue removal, *J Membr Sci* **430**, 2013, 96–105.

[112] X.Q. Cheng, L. Shao and C.H. Lau, High flux polyethylene glycol based nanofiltration membranes for water environmental remediation, *J Membr Sci* **476**, 2015, 95–104.

[113] Y. Liu, S. Zhang, Z. Zhou, J. Ren, Z. Geng, J. Luan, et al., Novel sulfonated thin-film composite nanofiltration membranes with improved water flux for treatment of dye solutions, *J Membr Sci* **394**, 2012, 218–229.

[114] Q. Yu, Y. Mao and X. Peng, Separation membranes constructed from inorganic nanofibers by filtration technique, *Chem Rec* **13**, 2013, 14–27.

[115] S. Karan, Q. Wang, S. Samitsu, Y. Fujii and I. Ichinose, Ultrathin free-standing membranes from metal hydroxide nanostrands, *J Membr Sci* **448**, 2013, 270–291.

[116] H. Wang, T.S. Chung and D.R. Paul, Physical aging and plasticization of thick and thin films of the thermally rearranged ortho-functional polyimide 6FDA–HAB, *J Membr Sci* **458**, 2014, 27–35.

[117] R.R. Tiwari, Z.P. Smith, H. Lin, B.D. Freeman and D.R. Paul, Gas permeation in thin films of “high free-volume” glassy perfluoropolymers: Part I. Physical aging, *Polymer* **55**, 2014, 5788–5800.

[118] C.H. Lau, K. Konstas, C.M. Doherty, S. Kanehashi, B. Ozcelik and S.E. Kentish, Tailoring physical aging in super glassy polymers with functionalized porous aromatic frameworks for CO_2 capture, *Chem Mater* **27**, 2015 4756–4762.

[119] J. Xia, T.S. Chung and D.R. Paul, Physical aging and carbon dioxide plasticization of thin polyimide films in mixed gas permeation, *J Membr Sci* **450**, 2014, 457–468.

[120] Y.H. Luo, J. Huang, J. Jin, X. Peng, W. Schmitt and I. Ichinose, Formation of positively charged copper hydroxide nanostrands and their structural characterization, *Chem Mater* **18**, 2006, 1795–1802.

[121] X. Peng, J. Jin, E.M. Ericsson and I. Ichinose, General method for ultrathin free-standing films of nanofibrous composite materials, *J Am Chem Soc* **129**, 2007, 8625–8633.

[122] X. Peng and I. Ichinose, Green-chemical synthesis of ultrathin β-MnOOH nanofibers for separation membranes, *Adv Func Mater* **21**, 2011, 2080–2087.

[123] X. Peng, J. Jin, N. Kobayashi, W. Schmitt and I. Ichinose, Time-dependent growth of zinc hydroxide nanostrands and their crystal structure, *Chem Commun* 2008, 1904–1906.

[124] K. Okada, R. Ricco, Y. Tokudome, M.J. Styles, A.J. Hill, M. Takahashi, et al., Copper conversion into Cu $(OH)_2$ nanotubes for positioning $Cu_3(BTC)_2$ MOF crystals: controlling the growth on flat plates, 3D architectures, and as patterns, *Adv Func Mater* **24**, 2014, 1969–1977.

[125] A.C. Yang, T.Y. Wang, C.A. Dai and D.Y. Kang, Incorporation of single-walled aluminosilicate nanotubes for the control of crystal size and porosity of zeolitic imidazolate framework-L, *Cryst Eng Comm* **18**, 2016, 881–887.

[126] T. Panda, T. Kundu and R. Banerjee, Self-assembled one dimensional functionalized metal–organic nanotubes (MONTs) for proton conduction, *Chem Commun* **48**, 2012, 5464–5466.

[127] F. Bu and S.J. Xiao, A 4-connected anionic metal–organic nanotube constructed from indium isophthalate, *Cryst Eng Commun* **12**, 2010, 3385–3387.

[128] X. Li, R. Wang, F. Wicaksana, C. Tang, J. Torres and A.G. Fane, Preparation of high performance nanofiltration (NF) membranes incorporated with aquaporin Z, *J Membr Sci* **450**, 2014, 181–188.

[129] K. Ariga, Silica-supported biomimetic membranes, *Chem Rec* **3**, 2004, 297–307.

[130] H. Wang, T.S. Chung, Y.W. Tong, K. Jeyaseelan, A. Armugam, Z. Chen, et al., Highly permeable and selective pore-spanning biomimetic membrane embedded with aquaporin Z, *Small* **8**, 2012, 1185–1190.

[131] M. Wang, Z. Wang, X. Wang, S. Wang, W. Ding and C. Gao, Layer-by-layer assembly of aquaporin Z-incorporated biomimetic membranes for water purification, *Environ Sci Technol* **49**, 2015, 3761–3768.

[132] Y.X. Shen, P.O. Saboe, I.T. Sines, M. Erbakan and M. Kumar, Biomimetic membranes: a review, *J Membr Sci* **454**, 2014, 359–381.

[133] A. Mecke, C. Dittrich and W. Meier, Biomimetic membranes designed from amphiphilic block copolymers, *Soft Matter* **2**, 2006, 751–759.

[134] J. Zhao, X. Zhao, Z. Jiang, Z. Li, X. Fan, J. Zhu, et al., Biomimetic and bioinspired membranes: preparation and application, *Prog Polym Sci* **39**, 2014, 1668–1720.

[135] H. Yu, X. Qiu, N. Moreno, Z. Ma, V.M. Calo and S.P. Nunes, Self-assembled asymmetric block copolymer membranes: bridging the gap from ultra-to nanofiltration, *Angew Chem Int Ed* **54**, 2015, 13937–13941.

[136] S. De Feyter and F.C. De Schryver, Two-dimensional supramolecular self-assembly probed by scanning tunneling microscopy, *Chem Soc Rev* **32**, 2003, 139–150, [177].

[137] Y. Lin, H. Skaff, T. Emrick, A.D. Dinsmore and T.P. Russell, Nanoparticle assembly and transport at liquid-liquid interfaces, *Science* **299**, 2003, 226–229.

[138] J. Zhao, F. Pan, P. Li, C. Zhao, Z. Jiang, P. Zhang, et al., Fabrication of ultrathin membrane via layer-by-layer self-assembly driven by hydrophobic interaction towards high separation performance, *ACS Appl Mater Interf* **5**, 2013, 13275–13283.

[139] R. Deng, S. Liu, J. Li, Y. Liao, J. Tao and J. Zhu, Mesoporous block copolymer nanoparticles with tailored structures by hydrogen-bonding-assisted self-assembly, *Adv Mater* **24**, 2012, 1889–1893.

[140] C.G. Claessens and J.F. Stoddart, Review commentary–interactions in self-assembly, *J Phys Org Chem* **10**, 1997, 254–272.

[141] F. Van Ackern, L. Krasemann and B. Tieke, Ultrathin membranes for gas separation and pervaporation prepared upon electrostatic self-assembly of polyelectrolytes, *Thin Solid Films* **327**, 1998, 762–766.

[142] L. Krasemann and B. Tieke, Ultrathin self-assembled polyelectrolyte membranes for pervaporation, *J Membr Sci* **150**, 1998, 23–30.

[143] L. Krasemann and B. Tieke, Composite membranes with ultrathin separation layer prepared by self-assembly of polyelectrolytes, *Mater Sci Eng C* **8**, 1999, 513–518.

[144] P. Van Rijn, M. Tutus, C. Kathrein, L. Zhu, M. Wessling and U. Schwaneberg, Challenges and advances in the field of self-assembled membranes, *Chem Soc Rev* **42**, 2013, 6578–6592.

[145] X. Qiu, H. Yu, M. Karunakaran, N. Pradeep, S.P. Nunes and K.V. Peinemann, Selective separation of similarly sized proteins with tunable nanoporous block copolymer membranes, *ACS Nano* **7**, 2012, 768–776.

[146] S.P. Nunes, A.R. Behzad, B. Hooghan, R. Sougrat, M. Karunakaran, N. Pradeep, et al., Switchable pH-responsive polymeric membranes prepared via block copolymer micelle assembly, *ACS Nano* **5**, 2011, 3516–3522.

[147] M. Gopinadhan, P. Deshmukh, Y. Choo, P.W. Majewski, O. Bakajin and M. Elimelech, Thermally switchable aligned nanopores by magnetic-field directed self-assembly of block copolymers, *Adv Mater* **26**, 2014, 5148–5154.

[148] W. Cheng, M.J. Campolongo, S.J. Tan and D. Luo, Freestanding ultrathin nano-membranes via self-assembly, *Nano Today* **4**, 2009, 482–493.

[149] C. Chen, Q.H. Yang, Y. Yang, W. Lv, Y. Wen and P.X. Hou, Self-assembled free-standing graphite oxide membrane, *Adv Mater* **21**, 2009, 3007–3011.

[150] J.J. Shao, W. Lv, Q. Guo, C. Zhang, Q. Xu and Q.H. Yang, Hybridization of graphene oxide and carbon nanotubes at the liquid/air interface, *Chem Commun* **48**, 2012, 3706–3708.

[151] L. Chen, L. Huang and J. Zhu, Stitching graphene oxide sheets into a membrane at a liquid/liquid interface, *Chem Commun* **50**, 2014, 15944–15947.

[152] Y. Lin, H. Skaff, A. Böker, A.D. Dinsmore, T. Emrick and T.P. Russell, Ultrathin cross-linked nanoparticle membranes, *J Am Chem Soc* **125**, 2003, 12690–12691.

[153] T. Huang, Q. An, X. Luan, Q. Zhang and Y. Zhang, Free-standing few-layered graphene oxide films: selective, steady and lasting permeation of organic molecules with adjustable speeds, *Nanoscale* **8**, 2016, 2003–2010.

[154] A.R. Koltonow and J.X. Huang, Two-dimensional nanofluidics, *Science* **351**, 2016, 1395–1396.

[155] R. Takekoh and T. Russell, Multi-length scale porous polymers, *Adv Func Mater* **24**, 2014, 1483–1489.

[156] B.K. Tripathi and P. Pandey, Breath figure templating for fabrication of polysulfone microporous membranes with highly ordered monodispersed porosity, *J Membr Sci* **471**, 2014, 201–210.

[157] C. Huang, T. Kamra, S. Chaudhary and X. Shen, Breath figure patterns made easy, *ACS Appl Mater Interf* **6**, 2014, 5971–5976.

[158] L.S. Wan, J.W. Li, B.B. Ke and Z.K. Xu, Ordered microporous membranes templated by breath figures for size-selective separation, *J Am Chem Soc* **134**, 2011, 95–98.

[159] J. Hahn, J.I. Clodt, C. Abetz, V. Filiz and V. Abetz, Thin isoporous block copolymer membranes: it is all about the process, *ACS Appl Mater Interf* **7**, 2015, 21130–21137.

[160] Y. Ou, C.J. Lv, W. Yu, Z.W. Mao, L.S. Wan and Z.K. Xu, Fabrication of perforated isoporous membranes via a transfer-free strategy: enabling high-resolution separation of cells, *ACS Appl Mater Interf* **6**, 2014, 22400–22407.

[161] Z. Wang, L. Guo and Y. Wang, Isoporous membranes with gradient porosity by selective swelling of UV-crosslinked block copolymers, *J Membr Sci* **476**, 2015, 449–456.

[162] Q.G. Zhang, C. Deng, R.R. Liu, Z. Lin, H.M. Li and A.M. Zhu, Ultrathin pH-sensitive nanoporous membranes for superfast size-selective separation, *Chem Asian J* **10**, 2015, 1133–1137.

[163] T. Femmer, A.J.C. Kuehne and M. Wessling, Print your own membrane: direct rapid prototyping of polydimethylsiloxane, *Lab Chip* **14**, 2014, 2610–2613.

[164] Z. Wang, J. Wang, M. Li, K. Sun and C.J. Liu, Three-dimensional printed acrylonitrile butadiene styrene framework coated with Cu-BTC metal-organic frameworks for the removal of methylene blue, *Sci Rep* **4**, 2014, 5939.

[165] T. Femmer, A. Kuehne, J. Torres-Rendon, A. Walther and M. Wessling, Print your membrane: rapid prototyping of complex 3D-PDMS membranes via a sacrificial resist, *J Membr Sci* **478**, 2015, 12–18.

[166] L. Wang, M. Fang, J. Liu, J. He, J. Li and J. Lei, Layer-by-layer fabrication of high-performance polyamide/ZIF-8 nanocomposite membrane for nanofiltration applications, *ACS Appl Mater Interf* **7**, 2015, 24082–24093.

[167] K. Huang, G. Liu, J. Shen, Z. Chu, H. Zhou, X. Gu, et al., High-efficiency water-transport channels using the synergistic effect of a hydrophilic polymer and graphene oxide laminates, *Adv Func Mater* **25**, 2015, 5809–5815.

[168] X. Lin, Q. Yang, L. Ding and B. Su, Ultrathin silica membranes with highly ordered and perpendicular nanochannels for precise and fast molecular separation, *ACS Nano* **9**, 2015, 11266–11277.

[169] K.C. Kao, C.H. Lin, T.Y. Chen, Y.H. Liu and C.Y. Mou, A general method for growing large area mesoporous silica thin films on flat substrates with perpendicular nanochannels, *J Am Chem Soc* **137**, 2015, 3779–3782.

[170] T.R. Gaborski, J.L. Snyder, C.C. Striemer, D.Z. Fang, M. Hoffman, P.M. Fauchet, et al., High-performance separation of nanoparticles with ultrathin porous nanocrystalline silicon membranes, *ACS Nano* **4**, 2010, 6973–6981.

[171] P. Van Rijn, M. Tutus, C. Kathrein, N.C. Mougin, H. Park and C. Hein, Ultra-thin self-assembled protein-polymer membranes: a new pore forming strategy, *Adv Func Mater* **24**, 2014, 6762–6770.

[172] J.S. Bae, E. Jeon, M. Byeon and J.W. Park, One-pot preparation of monolithic molecular separation membranes with sub-10 nm reticulated pores using concentration-polarization-induced gelation of covalent networ nanoparticles, *ACS Macro Lett* **4**, 2015, 991–995.

[173] C.E. Ren, K.B. Hatzell, M. Alhabeb, Z. Ling, K.A. Mahmoud and Y. Gogotsi, Charge-and size-selective ion sieving through Ti_3C_2T x MXene membranes, *J Phys Chem Lett* **6**, 2015, 4026–4031.

[174] C. Xu, A. Cui, Y. Xu and X. Fu, Graphene oxide–TiO_2 composite filtration membranes and their potential application for water purification, *Carbon* **62**, 2013, 465–471.

[175] N.F.D. Aba, J.Y. Chong, B. Wang, C. Mattevi and K. Li, Graphene oxide membranes on ceramic hollow fibers–microstructural stability and nanofiltration performance, *J Membr Sci* **484**, 2015, 87–94.

[176] X. Yao, J. Li, Z. Wang, L. Kong and Y. Wang, Highly permeable and robust membranes assembled from block-copolymer-functionalized carbon nanotubes, *J Membr Sci* **493**, 2015, 224–231.

[177] B. Lee, Y. Baek, M. Lee, D.H. Jeong, H.H. Lee and J. Yoon, A carbon nanotube wall membrane for water treatment, *Nat Commun* **6**, 2015, 7109.

[178] B. Tang, L. Zhang, R. Li, J. Wu, M.N. Hedhili and P. Wang, Are vacuum-filtrated reduced graphene oxide membranes symmetric, *Nanoscale* **8**, 2016, 1108–1116.

[179] K. Goh, W. Jiang, H.E. Karahan, S. Zhai, L. Wei and D. Yu, All-carbon nanoarchitectures as high-performance separation membranes with superior stability, *Adv Func Mater* **25**, 2015, 7348–7359.

[180] Q.G. Zhang, C. Deng, F. Soyekwo, Q.L. Liu and A.M. Zhu, Sub-10 nm wide cellulose nanofibers for ultrathin nanoporous membranes with high organic permeation, *Adv Func Mater* **26**, 2016, 792–800.

[181] A. Akbari, P. Sheath, S.T. Martin, D.B. Shinde, M. Shaibani and P.C. Banerjee, Large-area graphene-based nanofiltration membranes by shear alignment of discotic nematic liquid crystalls of graphene oxide, *Nat Commun* **7**, 2016, 10891.

[182] Z. Slouka, S. Senapati and H.C. Chang, Microfluidic systems with ion-selective membranes, *Ann Rev Anal Chem* **7**, 2014, 317–335.

[183] M.F. Jimenez-Solomon, Q. Song, K.E. Jelfs, M. Munoz-Ibanez and A.G. Livingston, Polymer nanofilms with enhanced microporosity by interfacial polymerization, *Nat Mater* **15**, 2016, 760–767.

[184] S. Karan, Z. Jiang and A.G. Livingston, Sub–10 nm polyamide nanofilms with ultrafast solvent transport for molecular separation, *Science* **348**, 2015, 1347–1351.

[185] Y. Zhang, J.L. Sargent, B.W. Boudouris and W.A. Phillip, Nanoporous membranes generated from self-assembled block polymer precursors: Quo Vadis, *J Appl Polym Sci* **132**, 2015, 41683.

[186] B. Sarkar and P. Alexandridis, Block copolymer–nanoparticle composites: structure, functional properties, and processing, *Prog Polym Sci* **40**, 2015, 33–62.

[187] T.N. Hoheisel, K. Hur and U.B. Wiesner, Block copolymer-nanoparticle hybrid self-assembly, *Prog Polym Sci* **40**, 2015, 3–32.

[188] Y. Gu, R.M. Dorin and U. Wiesner, Asymmetric organic–inorganic hybrid membrane formation via block copolymer–nanoparticle co-assembly, *Nano Lett* **13**, 2013, 5323–5328.

[189] C. Hörenz, C. Pietsch, A.S. Goldmann, C. Barne-Kowollik and F.H. Schacher, Phase inversion membranes from amphiphilic diblock terpolymers, *Adv Mater Interf* **2**, 2015, 15000042.

[190] P. Madhavan, K.V. Peinemann and S.P. Nunes, Complexation-tailored morphology of asymmetric block copolymer membranes, *ACS Appl Mater Interf* **5**, 2013, 7152–7159.

[191] H. Ahn, S. Park, S.W. Kim, P.J. Yoo, D.Y. Ryu and T.P. Russell, Nanoporous block copolymer membranes for ultrafiltration: a simple approach to size tunability, *ACS Nano* **8**, 2014, 11745–11752.

[192] Y. Gu and U. Wiesner, Tailoring pore size of graded mesoporous block copolymer membranes: moving from ultrafiltration toward nanofiltration, *Macromolecules* **48**, 2015, 6153–6159.

[193] H. Yu, X. Qiu, S.P. Nunes and K.V. Peinemann, Self-assembled isoporous block copolymer membranes with tuned pore sizes, *Angew Chem Int Ed* **53**, 2014, 10072–10076.

[194] H. Ma, C. Burger, B.S. Hsiao and B. Chu, Highly permeable polymer membranes containing directed channels for water purification, *ACS Macro Lett* **1**, 2012, 723–726.

[195] H.B. Soltane, D. Roizard and E. Favre, Effect of pressure on the swelling and fluxes of dense PDMS membranes in nanofiltration: an experimental study, *J Membr Sci* **435**, 2013, 110–119.

[196] L.E.M. Gevers, I.F.J. Vankelecom and P.A. Jacobs, Zeolite filled polydimethylsiloxane (PDMS) as an improved membrane for solvent-resistant nanofiltration (SRNF), *Chem Commun* 2005, 2500–2502.

[197] A. Dobrak-Van Berlo, I.F.J. Vankelecom and B. Van der Bruggen, Parameters determining transport mechanisms through unfilled and silicalite filled PDMS-based membranes and dense PI membranes in solvent resistant nanofiltration: comparison with pervaporation, *J Membr Sci* **374**, 2011, 138–149.

[198] C.H. Lau, P.T. Nguyen, M.R. Hill, A.W. Thornton, K. Konstas, C.M. Doherty, et al., Ending aging in super glassy polymer membranes, *Angew Chem Int Ed* **53**, 2014, 5322–5326.

[199] C.H. Lau, K. Konstas, A.W. Thornton, A.C. Liu, S. Mudie, D.F. Kennedy, et al., Gas-separation membranes loaded with porous aromatic frameworks that improve with age, *Angew Chem Int Ed* **54**, 2015, 2669–2673.

[200] X.Q. Cheng, K. Konstas, C.M. Doherty, C.D. Wood, X. Mulet, Z. Xie, et al., Organic microporous nanofillers with unique alcohol affinity for superior ethanol recovery toward sustainable biofuels, *Chemsuschem* **10**, 2017 1887–1891.

[201] X.Q. Cheng, K. Konstas, C.M. Doherty, C.D. Wood, X. Mulet, Z. Xie, et al., Hypercrosslinked additives that impede aging and enhance permeability in thin polyacetylene films for organic solvent nanofiltration, *ACS Appl Mater Interf* **9**, 2017, 14401–14408.

[202] X.Q. Cheng, S. Ding, J. Guo, C. Zhang, Z. Guo and L. Shao, In-situ interfacial formation of TiO2/polypyrrole selective layer for improving the separation efficiency towards molecular separation, *J Membr Sci* **536**, 2017 19–27.

[203] K.S. Novoselov, A.K. Geim, S.V. Morozov, D. Jiang, Y. Zhang and S.A. Dubonos, Electric field effect in atomically thin carbon films, *Science* **306**, 2004, 666–669.

[204] V. Nicolosi, M. Chhowalla, M.G. Kanatzidis, M.S. Strano and J.N. Coleman, Liquid exfoliation of layered materials, *Science* **340**, 2013, 1226419.

[205] J.N. Coleman, M. Lotya, A. O'Neill, S.D. Bergin, P.J. King and U. Khan, Two-dimensional nanosheets produced by liquid exfoliation of layered materials, *Science* **331**, 2011, 568–571.

[206] M. Chhowalla, H.S. Shin, G. Eda, L.J. Li, K.P. Loh and H. Zhang, The chemistry of two-dimensional layered transition metal dichalcogenide nanosheets, *Nat Chem* **5**, 2013, 263–275.

[207] M. Lotya, Y. Hernandez, P.J. King, R.J. Smith, V. Nicolosi and L.S. Karlsson, Liquid phase production of graphene by exfoliation of graphite in surfactant/water solutions, *J Am Chem Soc* **131**, 2009, 3611–3620.

[208] S. Park and R.S. Ruoff, Chemical methods for the production of graphenes, *Nat Nanotechnol* **4**, 2009, 217–224.

[209] Y. Hernandez, V. Nicolosi, M. Lotya, F.M. Blighe, Z. Sun and S. De, High-yield production of graphene by liquid-phase exfoliation of graphite, *Nat Nanotechnol* **3**, 2008, 563–568.

[210] R.J. Smith, P.J. King, M. Lotya, C. Wirtz, U. Khan and S. De, Large-scale exfoliation of inorganic layered compounds in aqueous surfactant solutions, *Adv Mater* **23**, 2011, 3944–3948.

[211] Q.H. Wang, K. Kalantar-Zadeh, A. Kis, J.N. Coleman and M.S. Strano, Electronics and optoelectronics of two-dimensional transition metal dichalcogenides, *Nat Nanotechnol* **7**, 2012, 699–712.

[212] R.F. Frindt, D. Yang and P. Westreich, Exfoliated single molecular layers of $Mn_{0.8}PS_3$ and $Cd_{0.8}PS_3$, *J Mater Res* **20**, 2005, 1107–1112.

[213] L. Wang, P. Brazis, M. Rocci, C.R. Kannewurf and M.G. Kanatzidis, A new redox host for intercalative polymerization: insertion of polyaniline into α-$RuCl_3$, *Chem Mater* **10**, 1998, 3298–3300.

[214] A. Takagaki, D. Lu, J.N. Kondo, M. Hara, S. Hayashi and K. Domen, Exfoliated HNb_3O_8 nanosheets as a strong protonic solid acid, *Chem Mater* **17**, 2005, 2487–2489.

[215] M. Osada, G. Takanashi, B.W. Li, K. Akatsuka, Y. Ebina, K. Ono, et al., Controlled polarizability of one-nanometer-thick oxide nanosheets for tailored, high-κ nanodielectrics, *Adv Func Mater* **21**, 2011, 3482–3487.

[216] T.J. Pinnavaia, Intercalated clay catalysts, *Science* **220**, 1983, 365–371.

[217] Q. Wu, A.O. Sjåstad, Ø.B. Vistad, K.D. Knudsen, J. Roots and J.S. Pedersen, Characterization of exfoliated layered double hydroxide (LDH, Mg/Al = 3) nanosheets at high concentrations in formamide, *J Mater Chem* **17**, 2007, 965–971.

[218] M. Naguib, O. Mashtalir, J. Carle, V. Presser, J. Lu and L. Hultman, Two-dimensional transition metal carbides, *ACS Nano* **6**, 2012, 1322–1331.

[219] M. Naguib, M. Kurtoglu, V. Presser, J. Lu, J. Niu and M. Heon, Two-dimensional nanocrystals produced by exfoliation of Ti_3AlC_2, *Adv Mater* **23**, 2011, 4248–4253.

[220] W.S. Hummers, Jr. and R.E. Offeman, Preparation of graphitic oxide, *J Am Chem Soc* **80**, 1958, 1339-9.

[221] D.R. Dreyer, S. Park, C.W. Bielawski and R.S. Ruoff, The chemistry of graphene oxide, *Chem Soc Rev* **39**, 2010, 228–240.

[222] C.J. Shih, A. Vijayaraghavan, R. Krishnan, R. Sharma, J.H. Han, M.H. Ham, et al., Bi-and trilayer graphene solutions, *Nat Nanotechnol* **6**, 2011, 439–445.

[223] G. Eda, H. Yamaguchi, D. Voiry, T. Fujita, M. Chen and M. Chhowalla, Photoluminescence from chemically exfoliated MoS_2, *Nano Lett* **11**, 2011, 5111–5116.

[224] P. Joensen, R.F. Frindt and S.R. Morrison, Single-layer MoS_2, *Mater Res Bull* **21**, 1986, 457–461.

[225] D. Voiry, H. Yamaguchi, J. Li, R. Silva, D.C. Alves, T. Fujita, et al., Enhanced catalytic activity in strained chemically exfoliated WS_2 nanosheets for hydrogen evolution, *Nat Mater* **12**, 2013, 850–855.

[226] R. Ma and T. Sasaki, Nanosheets of oxides and hydroxides: ultimate 2D charge-bearing functional crystallites, *Adv Mater* **22**, 2010, 5082–5104.

[227] G.F. Walker and W.G. Garrett, Chemical exfoliation of vermiculite and the production of colloidal dispersions, *Science* **156**, 1967, 385–387.

[228] J.N. Coleman, Liquid exfoliation of defect-free graphene, *Acc Chem Res* **46**, 2012, 14–22.

[229] M. Nomura, K. Ono, S. Gopalakrishnan, T. Sugawara and S.I. Nakao, Preparation of a stable silica membrane by a counter diffusion chemical vapor deposition method, *J Membr Sci* **251**, 2005, 151–158.

[230] S.B. Messaoud, A. Takagaki, T. Sugawara, R. Kikuchi and S.T. Oyama, Alkylamine–silica hybrid membranes for carbon dioxide/methane separation, *J Membr Sci* **477**, 2015, 161–171.

[231] G. Che, B.B. Lakshmi, E.R. Fisher and C.R. Martin, Carbon nanotubule membranes for electrochemical energy storage and production, *Nature* **393**, 1998, 346–349.

[232] S. Kitagawa, Metal–organic frameworks (MOFs), *Chem Soc Rev* **43**, 2014, 5415–5418.

[233] S. Qiu, M. Xue and G. Zhu, Metal–organic framework membranes: from synthesis to separation application, *Chem Soc Rev* **43**, 2014, 6116–6140.

[234] N. Stock and S. Biswas, Synthesis of metal-organic frameworks (MOFs): routes to various MOF topologies, morphologies, and composites, *Chem Rev* **112**, 2011, 933–969.

[235] A. Schneemann, V. Bon, I. Schwedler, I. Senkovska, S. Kaskel and R.A. Fischer, Flexible metal–organic frameworks, *Chem Soc Rev* **43**, 2014, 6062–6096.

[236] T. Rodenas, I. Luz, G. Prieto, B. Seoane, H. Miro and A. Corma, Metal–organic framework nanosheets in polymer composite materials for gas separation, *Nat Mater* **14**, 2015, 48–55.

[237] Y. Peng, Y. Li, Y. Ban, H. Jin, W. Jiao and X. Liu, Metal-organic framework nanosheets as building blocks for molecular sieving membranes, *Science* **346**, 2014, 1356–1359.

[238] L. Xu, X. Zhou, Y. Yu, W.Q. Tian, J. Ma and S. Lei, Surface-confined crystalline two-dimensional covalent organic frameworks via on-surface schiff-base coupling, *ACS Nano* **7**, 2013, 8066–8073.

[239] C.R. DeBlase, K. Hernández-Burgos, K.E. Silberstein, G.G. Rodríguez-Calero, R.P. Bisbey, H.D. Abruña, et al., Rapid and efficient redox processes within 2D covalent organic framework thin films, *ACS Nano* **9**, 2015, 3178–3183.

[240] T.Y. Zhou, S.Q. Xu, Q. Wen, Z.F. Pang and X. Zhao, One-step construction of two different kinds of pores in a 2D covalent organic framework, *J Am Chem Soc* **136**, 2014, 15885–15888.

[241] Y. Liu, Y. Ma, Y. Zhao, X. Sun, F. Gándara, H. Furukawa, et al., Weaving of organic threads into a crystalline covalent organic framework, *Science* **351**, 2016, 365–369.

[242] Q. Liu, Z. Tang, M. Wu and Z. Zhou, Design, preparation and application of conjugated microporous polymers, *Polym Int* **63**, 2014, 381–392.

[243] Y. Xu, S. Jin, H. Xu, A. Nagai and D. Jiang, Conjugated microporous polymers: design, synthesis and application, *Chem Soc Rev* **42**, 2013, 8012–8031.

[244] Y. Yuan, F. Sun, F. Zhang, H. Ren, M. Guo, K. Cai, et al., Targeted synthesis of porous aromatic frameworks and their composites for versatile, facile, efficacious, and durable antibacterial polymer coatings, *Adv Mater.* **25**, 2013, 6619–6624.

[245] T. Ben and S. Qiu, Porous aromatic frameworks: synthesis, structure and functions, *Cryst Eng Commun* **15**, 2013, 17–26.

[246] Y. Song, X. Li, C. Wei, J. Fu, F. Xu, H. Tan, et al., A green strategy to prepare metal oxide superstructure from metal-organic frameworks, *Sci Rep* **5**, 2015, 8401.

[247] J.Y. Lee, C.Y. Tang and F. Huo, Fabrication of porous matrix membrane (PMM) using metal-organic framework as green template for water treatment, *Sci Rep* **4**, 2014, 3740.

[248] J.A. Prince, S. Bhuvana, V. Anbharasi, N. Ayyanar, K.V.K. Boodhoo and G. Singh, Self-cleaning metal organic framework (MOF) based ultra filtration membranes-a solution to bio-fouling in membrane separation processes, *Sci Rep* **4**, 2014, 6555.

[249] J. Duan, Y. Pan, F. Pacheco, E. Litwiller, Z. Lai and I. Pinnau, High-performance polyamide thin-film-nanocomposite reverse osmosis membranes containing hydrophobic zeolitic imidazolate framework-8, *J Membr Sci* **476**, 2015, 303–310.

[250] S. Sorribas, P. Gorgojo, C. Téllez, J. Coronas and A.G. Livingston, High flux thin film nanocomposite membranes based on metal–organic frameworks for organic solvent nanofiltration, *J Am Chem Soc* **135**, 2013, 15201–15208.

[251] J. Campbell, G. Székely, R.P. Davies, D.C. Braddock and A.G. Livingston, Fabrication of hybrid polymer/metal organic framework membranes: mixed matrix membranes versus in situ growth, *J Mater Chem A* **2**, 2014, 9260–9271.

[252] S. Basu, M. Maes, A. Cano-Odena, L. Alaerts, D.E. De Vos and I.F. Vankelecom, Solvent resistant nanofiltration (SRNF) membranes based on metal-organic frameworks, *J Membr Sci* **344**, 2009, 190–198.

[253] Y. Li, L.H. Wee, A. Volodin, J.A. Martens and I.F. Vankelecom, Polymer supported ZIF-8 membranes prepared via an interfacial synthesis method, *Chem Commun* **51**, 2015, 918–920.

[254] J.H. Cavka, S. Jakobsen, U. Olsbye, N. Guillou, C. Lamberti, S. Bordiga, et al., A new zirconium inorganic building brick forming metal organic frameworks with exceptional stability, *J Am Chem Soc* **130**, 2008, 13850–13851.

[255] C.H. Lau, R. Babarao and M.R. Hill, A route to drastic increase of CO_2 uptake in Zr metal organic framework UiO-66, *Chem Commun* **49**, 2013, 3634–3636.

[256] M.J. Katz, Z.J. Brown, Y.J. Colón, P.W. Siu, K.A. Scheidt, R.Q. Snurr, et al., A facile synthesis of UiO-66, UiO-67 and their derivatives, *Chem Commun* **49**, 2013, 9449–9451.

[257] M. Kim, J.F. Cahill, H. Fei, K.A. Prather and S.M. Cohen, Postsynthetic ligand and cation exchange in robust metal-organic frameworks, *J Am Chem Soc* **134**, 2012, 18082–18088.

[258] M. Kandiah, S. Usseglio, S. Svelle, U. Olsbye, K.P. Lillerud and M. Tilset, Post-synthetic modification of the metal–organic framework compound UiO-66, *J Mater Chem* **20**, 2010, 9848–9851.

[259] K.M. Zwolinski, P. Nowak and M.J. Chmielewski, Towards multifunctional MOFs – transforming a side reaction into a post-synthetic protection/deprotection method, *Chem Commun* **51**, 2015, 10030–10033.

[260] S.J. Garibay and S.M. Cohen, Isoreticular synthesis and modification of frameworks with the UiO-66 topology, *Chem Commun* **46**, 2010, 7700–7702.

[261] K. Xie, Q. Fu, Y. He, J. Kim, S.J. Goh, E. Nam, et al., Synthesis of well dispersed polymer grafted metal–organic framework nanoparticles, *Chem Commun* **51**, 2015, 15566–15569.

[262] M. Henmi, K. Nakatsuji, T. Ichikawa, H. Tomioka, T. Sakamoto, M. Yoshio, et al., Self-organized liquid-crystalline nanostructured membranes for water treatment: selective permeation of ions, *Adv Mater* **24**, 2012, 2238–2241.

[263] T. Ichikawa, M. Yoshio, A. Hamasaki, J. Kagimoto, H. Ohno and T. Kato, 3D interconnected ionic nano-channels formed in polymer films: self-organization and polymerization of thermotropic bicontinuous cubic liquid crystals, *J Am Chem Soc* **133**, 2011, 2163–2169.

[264] B.M. Carter, B.R. Wiesenauer, E.S. Hatakeyama, J.L. Barton, R.D. Noble and D.L. Gin, Glycerol-based bicontinuous cubic lyotropic liquid crystal monomer system for the fabrication of thin-film membranes with uniform nanopores, *Chem Mater* **24**, 2012, 4005–4007.

[265] M. Zhou, P.R. Nemade, X. Lu, X. Zeng, E.S. Hatakeyama, R.D. Noble, et al., New type of membrane material for water desalination based on a cross-linked bicontinuous cubic lyotropic liquid crystal assembly, *J Am Chem Soc* **129**, 2007, 9574–9575.

[266] K. Ritos, M.K. Borg, D.A. Lockerby, D.R. Emerson and J.M. Reese, Hybrid molecular-continuum simulations of water flow through carbon nanotube membranes of realistic thickness, *Microfluid Nanofluid* **19**, 2015, 997–1010.

[267] S.C. O'Hern, D. Jang, S. Bose, J.C. Idrobo, Y. Song, T. Laoui, et al., Nanofiltration across defect-sealed nanoporous monolayer graphene, *Nano Lett* **15**, 2015, 3254–3260.

[268] T. Fujioka, N. Oshima, R. Suzuki, W.E. Price and L.D. Nghiem, Probing the internal structure of reverse osmosis membranes by positron annihilation spectroscopy: gaining more insight into the transport of water and small solutes, *J Membr Sci* **486**, 2015, 106–118.

[269] X. Meng and J. Huang, Enhancement of water flow across a carbon nanotube, *Mol Simulat* **42**, 2016, 215–219.

[270] S.C. Chen, G.L. Amy and T.S. Chung, Membrane fouling and anti-fouling strategies using RO retentate from a municipal water recycling plant as the feed for osmotic power generation, *Water Res* **88**, 2016, 144–155

[271] A. Walther and A.H.E. Müller, Janus particles: synthesis, self-assembly, physical properties, and applications, *Chem Rev* **113**, 2013, 5194–5261.

[272] X. Tian, H. Jin, J. Sainio, R.H. Ras and O. Ikkala, Droplet and fluid gating by biomimetic Janus membranes, *Adv Func Mater* **24**, 2014, 6023–6028.

[273] H. Wang, H. Zhou, H. Niu, J. Zhang, Y. Du and T. Lin, Superamphiphobic/superhydrophobic-oleophilic nanofibrous membranes with unidirectional oil-transport ability and strengthened oil-water separation performance, *Adv Mater Interf* **2**, 2015, 1400506.

[274] H.C. Yang, J. Hou, V. Chen and Z.K. Xu, Janus membranes: exploring duality for advanced separation, *Angew Chem Int Ed* **55**, 2016, 13398–13407.

[275] Z.X. Wang, X.B. Yang, Z.J. Cheng, Y.Y. Liu, L. Shao and L. Jiang, Simply realizing ''water diode'' Janus membranes for multifunctional smart applications, *Mater Horizons* **4**, 2017, 701–708.

[276] H.C. Yang, J. Hou, L.S. Wan, V. Chen and Z.K. Xu, Janus membranes with asymmetric wettability for fine bubble aeration, *Adv Mater Interf* **3**, 2016, 1500774.

Queries and Answers

Query: Your article is registered as a regular item and is being processed for inclusion in a regular issue of the journal. If this is NOT correct and your article belongs to a Special Issue/Collection please contact san.natarajan@elsevier.com immediately prior to returning your corrections.
Answer: Yes. It is the regular item.

Query: The author names have been tagged as given names and surnames (surnames are highlighted in teal color). Please confirm if they have been identified correctly.
Answer: All are correct.

Query: Please check the address for the corresponding authors that have been added here, and correct if necessary.
Answer: It is not correct. I have inserted the correct words.

Query: One or more sponsor names may have been edited to a standard format that enables better searching and identification of your article. Please check and correct if necessary.
Answer: All are right.

Query: Please check the year in Refs. [33,136].
Answer: There is no problem for any reference regarding the publishing year.

Query: Please check the edit(s) made in Table 1, and correct if necessary.
Answer: All are correct. Thanks